Research Article

Marko Mlikota* and Frank Schorfheide*

Sequential Monte Carlo With Model Tempering

https://doi.org/10.1515/sample-YYYY-XXXX
Received Month DD, YYYY; revised Month DD, YYYY; accepted Month DD, YYYY

Abstract: Modern macroeconometrics often relies on time series models for which it is time-consuming to evaluate the likelihood function. We demonstrate how Bayesian computations for such models can be drastically accelerated by reweighting and mutating posterior draws from an approximating model that allows for fast likelihood evaluations, into posterior draws from the model of interest, using a sequential Monte Carlo (SMC) algorithm. We apply the technique to the estimation of a vector autoregression with stochastic volatility and two nonlinear dynamic stochastic general equilibrium models. The runtime reductions we obtain range from 27% to 88%.

Keywords: Bayesian Computations, Dynamic Stochastic General Equilibrium Models, Sequential Monte Carlo, Stochastic Volatility, Vector Autoregressions

1 Introduction

Modern macroeconometrics often relies on time series models for which it is time-consuming to evaluate the likelihood function, either because it takes a long time to solve the underlying structural model, or the likelihood evaluation requires to integrate out latent state variables. In this paper we demonstrate how Bayesian computations for such models can be accelerated by reweighting and mutating posterior draws from an approximating model that allows for fast likelihood evaluations. We show that a sequential Monte Carlo (SMC) algorithm that starts out with draws from the posterior distribution of an approximating model instead of the prior distribution of the target model can drastically speed up the posterior computations.

SMC methods have been traditionally used to solve nonlinear filtering problems, an example being the bootstrap particle filter of Gordon et al. (1993). Subsequently, Chopin (2002) showed how to adapt particle filtering techniques to conduct posterior inference for a static parameter vector. SMC methods are widely used in statistics; see Dai et al. (2022) for a recent review. They also have emerged in certain branches of the econometrics literature. The first paper that applied SMC techniques to posterior inference for the parameters of a (small-scale) DSGE model was Creal (2007). Subsequent work by Herbst and Schorfheide (2014, 2015) fine-tuned the algorithm so that it could be used for the estimation of medium- and large-scale models. Durham and Geweke (2014) show how to parallelize a flexible and self-tuning SMC algorithm for the estimation of time series models on graphical processing units (GPU).

In general, SMC algorithms approximate a target posterior distribution by creating intermediate approximations to a sequence of bridge distributions, indexed in this paper by n. At each stage, the current bridge distribution is represented by a swarm of so-called particles. Each particle is composed of a value and a weight. Weighted averages of the particle values converge to expectations under the stage-n distribution. The transition from stage $n-1$ to n involves changing the particle weights and values (mutation) so that the swarm adapts to the new distribution. Typically, these bridge distributions are constructed by either using the full-sample likelihood (*likelihood tempering*, LT)—generated by raising this likelihood function

***Corresponding author: Marko Mlikota,** University of Pennsylvania, Department of Economics, Philadelphia, U.S.A., e-mail: mlikota@sas.upenn.edu
Frank Schorfheide*, University of Pennsylvania, Department of Economics, Philadelphia, U.S.A., e-mail: schorf@upenn.edu

to the power of ϕ_n, where ϕ_n increases from zero to one—or by sequentially adding observations to the likelihood function (*data tempering*, DT).

In this paper we propose a *model tempering approach* that takes a geometric average with weights ϕ_n and $1-\phi_n$ of the likelihood functions associated with the target model, denoted by M_1, and an approximating model M_0. We document the achievable runtime reductions in various applications. In one of the applications M_1 and M_0 are vector autoregressions (VARs) with and without stochastic volatility (SV). In another application we consider a nonlinear and a linearized version of a DSGE model. In the econometrics literature Doppelt and O'Hara (2020) used a version of model tempering to estimate a fractionally-integrated VAR based on an approximate and an exact likelihood function. However, the paper does not study the runtime and accuracy properties in detail and the initialization is based on Markov chain Monte Carlo (MCMC) instead of SMC draws, which complicates the theoretical analysis of the algorithm considerably. Cai et al. (2021) discuss potential benefits of model tempering without implementing it, and Acharya et al. (2021) discuss model tempering as a strategy to estimate a heterogeneous agent New Keynesian model, starting from a simpler representative agent model.

In general, model tempering is an attractive computational strategy for applications in which the likelihood evaluation for the target model is computationally costly and there is an approximating model for which the likelihood evaluation is fast and generates a posterior that is not too different from the posterior of the target model. We envision the approximating model to be a simplified version of the target model for which posterior computations are also implemented via SMC, in this case with likelihood tempering.[1]

We propose two important refinements to a general model tempering approach that may improve the performance in practice and broaden its applicability. First, the M_0 likelihood tempering can be terminated before the weight on the likelihood function has reached the value one. We denote the terminal weight on the M_0 likelihood by $\psi_* \in (0,1]$. The early termination will lead to a more diffuse M_0 posterior, draws from which might be more easily mutable into draws from the M_1 posterior in the subsequent model tempering steps. This feature introduces additional flexibility into the model tempering algorithm. A desirable degree of M_0 tempering can be assessed *ex ante* by examining the variance of importance weights that are required to convert M_0 draws into M_1 draws. Second, our algorithm can handle applications in which the parameter spaces for M_0 and M_1 are not exactly identical.

Building on earlier work in the statistics literature, e.g., Jasra et al. (2011), Del Moral et al. (2012), Schäfer and Chopin (2013), Geweke and Frischknecht (2014), and Zhou et al. (2015), and work in the DSGE model literature, e.g., Herbst and Schorfheide (2019) and Cai *et al.* (2021), we choose the tempering schedule defined through the ϕ_n sequence adaptively. Our adaptive schedules are calibrated by a single tuning parameter that controls the desired variance of the particle weights. The smaller the discrepancy between the posterior distribution of the approximating and the original model, the fewer bridge distributions are being used, and the faster the posterior analysis.

We provide a formula for the runtime reduction achievable by model tempering that depends on the number of stages as a function of ψ_* used for the M_0 and M_1 SMC runs, respectively, and the relative time it takes to evaluate the likelihood functions of the two models, denoted by the ratio τ_0/τ_1. Note that the user can evaluate τ_0/τ_1 before running the entire algorithm. We show that the runtime reduction profile is convergent as $\tau_0/\tau_1 \longrightarrow 0$. In the limit, the runtime reduction is determined just by the number of M_0 and M_1 SMC stages, which in turn depends on the alignment of the ψ_*-tempered M_0 posterior and the target M_1 posterior, relative to the alignment of the prior and the M_1 posterior. To assess the potential gains of model tempering *ex ante*, we recommend that the researcher computes the variance of the importance sampling weights, that would be needed to reweight the draws from the ψ_*-tempered M_0 posterior to approximate the target M_1 posterior, for various choices of ψ_*. If there is a ψ_* for which this variance is small relative to the number of SMC particles, then the gains from model tempering are potentially large.

[1] Even in the absence of a model tempering strategy, estimating approximating models is desirable as part of the modeling and code debugging that ultimately leads to the target model.

We consider several numerical illustrations of model tempering. In the first illustration, both target and approximating densities are univariate Normal. We illustrate how the distance between the densities affects the number of stages (and computational time) required to convert draws from the approximating density into draws from the target density. In the second illustration we consider the estimation of a VAR with SV, using a homoskedastic VAR as approximating model. In our illustration, model tempering is able to reduce the computational time by 79%. At last we consider the estimation of two dynamic stochastic general equilibrium (DSGE) models. We take M_1 as a version of the model that is solved with a second-order perturbation around the steady state and for which the likelihood function is evaluated with a bootstrap particle filter (BSPF). The approximating model is a log-linearized version for which the likelihood function can be evaluated quickly using the Kalman filter. In our application to the estimation of a real business cycle (RBC) model, model tempering can reduce the runtime of our JULIA code from 655 to 80 minutes.

The idea of using an approximating model as part of a Monte Carlo strategy is, of course, an old one. In fact, classic importance sampling as in Kloek and van Dijk (1978) is based on the notion that there is an alternative distribution available, possibly from an approximating model, from which one can sample directly and then reweight the draws. Unfortunately, in many applications it is difficult to construct an approximating density that mimics the target density which leads to inaccurate Monte Carlo approximations. SMC constructs the approximating density sequentially using a tempering strategy. As an alternative, Hoogerheide et al. (2012) proposed to approximate the target density by a mixture of Student-t distribution. Here the challenge is to compute the appropriate mixture weights.

Approximating models have also been used in Metropolis-Hastings algorithms to create surrogate transitions or delayed acceptances. The basic idea is to first evaluate a sequence of proposed draws under an approximating model that allows for a fast likelihood computation to increase the probability that the final proposal, evaluated under the target posterior, will be accepted; see, for instance, Liu (2001) and Christen and Fox (2005) for general approaches, and Smith (2011) for an adaption to the estimation of DSGE models. Bon et al. (2021) incorporate the delayed acceptance into the mutation step of an SMC sampler. Finally, approximating models are also often used in particle filters to construct proposal distributions that are adapted to next period's observation, e.g., Kim et al. (1998) and, in the DSGE model context, the approximately conditionally optimal proposals discussed in Herbst and Schorfheide (2015).

The remainder of this paper is organized as follows. Section 2 describes the proposed model tempering SMC algorithm. Section 3 considers the simple example based on univariate Gaussian posterior distributions. In Section 4 we use model tempering to estimate the VAR with SV. In Section 5 we implement our algorithm to estimate two nonlinear DSGE model: an RBC model and a New Keynesian DSGE model with asymmetric price and wage adjustment costs. Section 6 concludes. An Online Appendix contains supplemental information on the methodology and further details and results for the numerical illustrations. Replication codes and instructions of how to adapt these codes to other models are provided at Marko Mlikota's github site https://github.com/markomlikota/SMC-MT.

2 Bayesian Inference, SMC, and Model Tempering

VARs, DSGE models, and other time series models are often estimated using Bayesian inference for several reasons. First, the Bayesian framework provides a powerful toolkit to handle the presence of latent variables in state-space models. Second, uncertainty about parameters, shocks, and unobserved state variables is treated identically which makes it conceptually straightforward to form predictive distributions that reflect all sources of uncertainty. Third, prior distributions can be used to regularize the estimation of high-dimensional models (e.g., VARs) or to incorporate additional information not contained in the estimation sample (DSGE model estimation).

Fig. 1: Evolution of Bridge Distributions

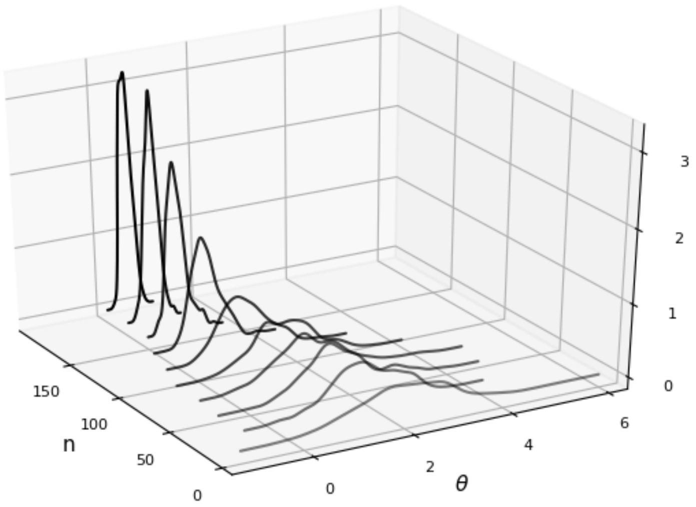

Notes: The sequence of bridge distributions for a scalar parameter θ is shown along the y-axis.

Bayesian inference combines a prior distribution $p(\theta)$ with a likelihood function $p(Y|\theta)$ to form a posterior distribution $p(\theta|Y)$, which is given by

$$\pi(\theta) \equiv p(\theta|Y) = \frac{p(Y|\theta)p(\theta)}{p(Y)}, \quad p(Y) = \int p(Y|\theta)p(\theta)d\theta, \tag{1}$$

where $Y = Y_{1:T} = \{y_1, y_2, ..., y_T\}$ and the normalization constant $p(Y)$ is called the marginal data density (MDD). In most applications, the posterior distribution $p(\theta|Y)$ does not belong to a family of distributions for which moments and percentiles can be easily calculated or draws can be obtained by direct sampling. In this paper we use an SMC algorithm to sample from the posterior distribution $p(\theta|Y)$. The algorithm combines insights from importance sampling and Markov chain Monte Carlo (MCMC) techniques. Two of its key advantages are that it is able to provide accurate approximations of non-regular posterior distributions[2] and that it can be easily parallelized, unlike MCMC algorithms. In Section 2.1 we describe a generic SMC algorithm to sample from the posterior distribution of θ. The section draws heavily from the more detailed exposition in Herbst and Schorfheide (2014, 2015). Model tempering, which is the focus of our paper, is introduced in Section 2.2 and implementation details are discussed in Section 2.3. In Section 2.4 we assess potential runtime reductions.

2.1 A Generic SMC Algorithm

In order to draw from $\pi(\theta)$, the SMC algorithm uses a sequence of bridge posterior distributions $\{\pi_n(\theta)\}_{n=0}^{N_\phi}$, illustrated in Figure 1, where the last one in the sequence equals the posterior distribution – $\pi_{N_\phi}(\theta) = \pi(\theta)$ – and where each $\pi_{n-1}(\theta)$ is used as the proposal density for $\pi_n(\theta)$. The bridge posteriors are constructed

[2] Herbst and Schorfheide (2014) document empirically in the context of the Smets and Wouters (2007) model with a diffuse prior, that the SMC algorithm is able to capture the multimodality of the posterior distribution much better than a Metropolis-Hastings algorithm. Mathews and Schmidler (2022) show theoretically through finite-sample accuracy bounds that when target distributions are multimodal, global mixing of the Markov kernel may be slow and SMC is preferable over MCMC.

from stage n likelihood functions $p_n(Y|\theta)$ and defined as

$$\pi_n(\theta) = \frac{p_n(Y|\theta)p(\theta)}{\int p_n(Y|\theta)p(\theta)d\theta}. \tag{2}$$

Each density $\pi_n(\theta)$ is represented by a particle approximation $\{\theta_n^i, W_n^i\}_{i=1}^N$. Thus, at stage n the algorithm propagates the particles $\{\theta_{n-1}^i, W_{n-1}^i\}_{i=1}^N$ so that they come to represent the target density $\pi_n(\theta)$. Formally, the algorithm proceeds in the following steps:

Algorithm 1 (Generic SMC Algorithm).

1. **Initialization.** *($n = 0$ and $\phi_0 = 0$.) Draw the initial particles from $\pi_0(\theta)$: $\theta_1^i \sim \pi_0(\theta)$ and $W_1^i = 1$, $i = 1, \ldots, N$.*
2. **Recursion.** *For $n = 1, \ldots, N_\phi$,*
   (a) **Correction.** *Reweight the particles from stage $n-1$ by defining the incremental weights*

   $$\tilde{w}_n^i = \frac{p_n(Y|\theta_{n-1}^i)}{p_{n-1}(Y|\theta_{n-1}^i)} \tag{3}$$

   and the normalized weights

   $$\tilde{W}_n^i = \frac{\tilde{w}_n^i W_{n-1}^i}{\frac{1}{N}\sum_{i=1}^N \tilde{w}_n^i W_{n-1}^i}, \quad i = 1, \ldots, N. \tag{4}$$

   (b) **Selection (Optional).** *Resample the swarm of particles, $\{\theta_{n-1}^i, \tilde{W}_n^i\}_{i=1}^N$, and denote resampled particles by $\{\hat{\theta}_n^i, W_n^i\}_{i=1}^N$, where $W_n^i = 1$ for all i.*
   (c) **Mutation.** *Starting from $\hat{\theta}_n^i$, propagate the particles $\{\hat{\theta}_n^i, W_n^i\}$ via N_{MH} steps of a Metropolis-Hastings (MH) algorithm with transition density $K_n(\theta|\tilde{\theta};\zeta_n)$ and stationary distribution $\pi_n(\theta)$. Note that the weights are unchanged, and denote the mutated particles by $\{\theta_n^i, W_n^i\}_{i=1}^N$.*

   An approximation of $\mathbb{E}_{\pi_n}[h(\theta)]$ is given by

   $$\bar{h}_{n,N} = \frac{1}{N}\sum_{i=1}^N h(\theta_n^i)W_n^i. \tag{5}$$

3. *For $n = N_\phi$ ($\phi_{N_\phi} = 1$) the final importance sampling approximation of $\mathbb{E}_\pi[h(\theta)]$ is given by:*

   $$\bar{h}_{N_\phi,N} = \sum_{i=1}^N h(\theta_{N_\phi}^i)W_{N_\phi}^i. \tag{6}$$

The correction step is a classic importance sampling step, in which the particle weights are updated to reflect the stage n distribution $\pi_n(\theta)$. The selection step is optional. On the one hand, resampling adds noise to the Monte Carlo approximation, which is undesirable. On the other hand, it equalizes the particle weights, which increases the accuracy of subsequent importance sampling approximations. The decision of whether or not to resample is typically based on a threshold rule for the variance of the particle weights which can be transformed into an effective particle sample size (ESS):

$$\widehat{ESS}_n = N\Big/\left(\frac{1}{N}\sum_{i=1}^N (\tilde{W}_n^i)^2\right). \tag{7}$$

If the particles have equal weights, then $\widehat{ESS}_n = N$. If one particle has weight N and all other particles have weight 0, then $\widehat{ESS}_n = 1$. These are the upper and lower bounds for the effective sample size. To balance the trade-off between adding noise and equalizing particle weights, we execute the resampling step if $\widehat{ESS}_n$ falls below $N/2$ using a systematic resampling algorithm.

The mutation step changes the particle values. In the absence of the mutation step, the particle values would be restricted to the set of values drawn in the initial stage from the prior distribution. This would clearly be inefficient, because the prior distribution is typically a poor proposal distribution for the posterior in an importance sampling algorithm. As the algorithm cycles through the N_ϕ stages, the particle values successively adapt to the shape of the posterior distribution. This is the key difference between SMC and classic importance sampling. The transition kernel $K_n(\theta|\tilde{\theta};\zeta_n)$ is designed to have the following invariance property:

$$\pi_n(\theta_n) = \int K_n(\theta_n|\hat{\theta}_n;\zeta_n)\pi_n(\hat{\theta}_n)d\hat{\theta}_n. \tag{8}$$

Thus, if $\hat{\theta}_n^i$ is a draw from π_n, then so is θ_n^i. The mutation step can be implemented by using one or more steps of a MH algorithm. The probability of mutating the particles can be increased by blocking the elements of the parameter vector θ or by iterating the MH algorithm over multiple steps. The vector ζ_n summarizes the tuning parameters of the MH algorithm.

2.2 Model Tempering

Up to now we imposed minimal conditions on the sequence of bridge posterior distributions. To initialize the algorithm, we implicitly required that it is possible to sample from the initial distribution $\pi_0(\theta)$, which is typically the prior $p(\theta)$ under likelihood or data tempering, and we required that the stage N_ϕ posterior is equal to the target posterior distribution: $\pi_{N_\phi}(\theta) = \pi(\theta)$. While previous applications of Algorithm 1 in econometrics focused on either data or likelihood tempering, the contribution of our paper is to assess the performance of the model tempering approach. Under model tempering the bridge distributions are constructed as follows. Let M_1 be the target model with likelihood function $p(Y|\theta, M_1)$ and let M_0 be an approximating model with likelihood function $p(Y|\theta, M_0)$. We define the bridge likelihood functions that are used in Steps 2(a) and 2(c) of Algorithm 1 as:

$$p_n(Y|\theta) = p(Y|\theta, M_1)^{\phi_n} p(Y|\theta, M_0)^{1-\phi_n}\ , \quad \phi_0 = 0, \quad \phi_{N_\phi} = 1, \quad \phi_n \uparrow 1. \tag{9}$$

It can be easily seen that $\pi_{N_\phi}(\theta) = p(\theta|Y, M_1)$, as required, and that the algorithm is initialized with draws from the M_0 posterior $\pi_0(\theta) = p(\theta|Y, M_0)$. The intermediate distributions are obtained by shifting the weight gradually from the M_0 posterior to the posterior of the target model M_1.

Model tempering distinguishes itself from the two most widely-used tempering schemes, likelihood tempering and data tempering, neither of which involve an approximating model M_0. Under likelihood tempering (e.g., Herbst and Schorfheide (2014)) the stage n posterior is constructed from a tempered version of the full-sample likelihood function:

$$p_n(Y|\theta) = p(Y|\theta, M_1)^{\phi_n}.$$

Under data tempering (e.g., Durham and Geweke (2014)) the bridge distributions are obtained from a fraction of the sample observations $\pi_n(\theta) \propto p(Y_{1:\lfloor\phi_n T\rfloor}|\theta, M_1)p(\theta)$ or, as in Cai *et al.* (2021), by gradually shifting the weight from a short-sample likelihood to a full-sample likelihood:

$$p_n(Y|\theta) = p(Y_{1:T}|\theta, M_1)^{\phi_n} p(Y_{1:T_0}|\theta, M_1)^{1-\phi_n}, \quad T_0 < T.$$

Model tempering is a computationally efficient alternative under two conditions. First, the likelihood evaluation of the target model M_1 is computationally costly, whereas the likelihood evaluation of the approximating model M_0 is, in relative terms, fast. Second, the likelihood functions of the target and the approximating model have to be sufficiently close such that only a modest number of intermediate stages are required to convert draws from the M_0 posterior into draws from the M_1 posterior. We provide a more detailed discussion in Section 2.4 below.

2.3 Implementation Details

Adaptive Tempering Schedule. Under the adaptive tempering schedule used in Cai *et al.* (2021) ϕ_n is chosen to target a desired level of the ESS defined in (7). Emphasizing the dependence of the incremental weights on the current tempering coefficient ϕ, write $\tilde{w}_n^i$ in (3) as

$$\tilde{w}^i(\phi) = \frac{p(Y|\theta^i_{n-1}, M_1)^{\phi} p(Y|\theta^i_{n-1}, M_0)^{1-\phi}}{p(Y|\theta^i_{n-1}, M_1)^{\phi_{n-1}} p(Y|\theta^i_{n-1}, M_0)^{1-\phi_{n-1}}}$$

and define

$$f(\phi) = \widehat{ESS}_n(\phi) - \alpha \widehat{ESS}^*_{n-1}, \quad 0 < \underline{\alpha} \leq \alpha < 1,$$

where $\widehat{ESS}^*_{n-1} = \widehat{ESS}_{n-1}$ if the stage $n-1$ selection step (resampling) was executed and $\widehat{ESS}^*_{n-1} = N$ otherwise. Let ϕ_n^* satisfy $f(\phi_n^*) = 0$ and define $\phi_n = \min\{\phi_n^*, 1\}$.

The parameter α, to be specified by the user, is the targeted reduction in ESS. It can be shown that for $\phi > \phi_{n-1}$ the ESS satisfies the inequality $\widehat{ESS}_n(\phi) < \widehat{ESS}^*_{n-1}$. Moreover, $\widehat{ESS}_n(\phi)$ is a strictly decreasing function of ϕ such that $f(\phi) = 0$ has a unique solution. The adaptive algorithm chooses the tempering schedule to control the deterioration of the ESS statistic. The smaller the slope of the function $\widehat{ESS}_n(\phi)$, the larger the increments in the tempering schedule. The number of stages N_ϕ and runtime are then endogenously determined by the closeness of $\pi_0(\theta)$ and $\pi(\theta)$. The number of stages is equal to the stage n at which $\phi_n = 1$.

Model-Specific Parameters. It might be the case that not all of the parameters that appear in M_1 also affect M_0, or vice versa. For instance, in one of our illustrations, M_1 is a VAR with SV, whereas M_0 is a homoskedastic VAR. Thus, the M_1 parameter vector contains additional parameters that govern the dynamics of the SV processes. Partition $\theta' = [\theta_c', \theta_0', \theta_1']$, where θ_c is the vector of common parameters and θ_j are parameters specific to model M_j. The likelihood functions are given by

$$p(Y|\theta, M_j) = p(Y|\theta_c, \theta_j, M_j), \quad j = 0, 1$$

and

$$p_n(Y|\theta) = p(Y|\theta_c, \theta_1, M_1)^{\phi_n} p(Y|\theta_c, \theta_0, M_0)^{1-\phi_n}. \tag{10}$$

Consider stage $n = 0$ with $\phi_0 = 0$. Because θ_1 does not enter the M_0 likelihood function, its distribution does not get updated in view of the data Y and we can factorize the M_0 posterior as follows.

$$\pi_0(\theta) = p(\theta|Y, M_0) = p(\theta_c, \theta_0|Y, M_0) p(\theta_1).$$

Thus, the model tempering SMC algorithm starts from posterior draws of (θ_c, θ_0) and prior draws from θ_1. The use of prior draws for θ_1 in the absence from any information through M_0 is both natural and desirable.

At stage $n = N_\phi$ the SMC algorithm approximates the M_1 posterior which, on the enlarged parameter space, is given by

$$\pi_{N_\phi}(\theta) = p(\theta|Y, M_1) = p(\theta_c, \theta_1|Y, M_1) p(\theta_0).$$

The ultimate object of interest is, in slight abuse of notation, the marginal posterior

$$p(\theta_c, \theta_1|Y, M_1) = \int \pi_{N_\phi}(\theta_c, \theta_0, \theta_1) d\theta_0.$$

While the SMC sampler generates draws from the joint posterior of $(\theta_c, \theta_0, \theta_1)$, draws from the marginal posterior can be obtained by simply dropping the θ_0 draws. A potential disadvantage of including θ_0 into the definition of θ is that the SMC algorithm has to turn θ_0 draws from a potentially highly concentrated posterior $p(\theta_0|Y, M_0)$ into draws from a more diffuse prior $p(\theta_0)$, which may require an undesirably large number of steps. Thus, we recommend to simply fix θ_0 at a reasonable value, e.g., the posterior mean or mode from a preliminary estimation of M_0, and then drop it from the definition of θ.

Marginal Data Density Ratio. The SMC algorithm produces as a by-product an approximation of the marginal likelihood ratio $p(Y|M_1)/p(Y|M_0)$. Note that

$$\frac{1}{N}\sum_{i=1}^{N} \tilde{w}_n^i \tilde{W}_{n-1}^i \approx \int \frac{p_n(Y|\theta)}{p_{n-1}(Y|\theta)} \left[\frac{p_{n-1}(Y|\theta)p(\theta)}{\int p_{n-1}(Y|\theta)p(\theta)d\theta}\right] d\theta = \frac{\int p_n(Y|\theta)p(\theta)d\theta}{\int p_{n-1}(Y|\theta)p(\theta)d\theta}, \tag{11}$$

where

$$\begin{aligned}\int p_0(Y|\theta)p(\theta)d\theta &= \int p(Y|\theta, M_0)p(\theta)d\theta = p(Y|M_0) \\ \int p_{N_\phi}(Y|\theta)p(\theta)d\theta &= \int p(Y|\theta, M_1)p(\theta)d\theta = p(Y|M_1).\end{aligned}$$

In turn, it can be shown that

$$\prod_{n=1}^{N_\phi}\left(\frac{1}{N}\sum_{i=1}^{N}\tilde{w}_n^i W_{n-1}^i\right) \overset{\text{a.s.}}{\longrightarrow} \frac{p(Y|M_1)}{p(Y|M_0)} \tag{12}$$

as the number of particles $N \longrightarrow \infty$; see, for instance, Herbst and Schorfheide (2014).

Tempered M_0 Posterior. Rather than using the full-information posterior under M_0 as the proposal density, one can choose to incorporate only a fraction of the information embodied in the posterior under model M_0. Suppose that the draws from M_0 are generated through an SMC algorithm with likelihood tempering, which is what we are doing in the illustrations in Sections 4 and 5. Then we can define

$$p_n(Y|\theta) = p(Y|\theta, M_1)^{\phi_n}\left[p(Y|\theta, M_0)^{\psi_*}\right]^{1-\phi_n}, \quad \psi_* \in [0, 1)\ , \tag{13}$$

which leads to the initialization

$$\pi_0(\theta;\psi_*) \propto p(Y|\theta, M_0)^{\psi_*}p(\theta)\ . \tag{14}$$

The density $\pi_0(\theta;\psi_*)$ represents the posterior obtained from the tempered M_0 likelihood function. Thus, the posterior sampling for the approximating model is terminated at $\phi_{N_\phi} = \psi_* < 1$ instead of $\phi_{N_\phi} = 1$. The advantage of this strategy is that for $\psi_* < 1$ the density $\pi_0(\theta;\psi_*)$ is more diffuse than the full M_0 posterior and may exhibit a greater overlap with the target posterior in applications in which M_0 and M_1 posteriors differ substantially. Note that for $\psi_* = 0$ the model M_1 would be estimated by standard likelihood tempering instead of model tempering.

2.4 Computational Gains

To formalize the discussion of the computational advantage of model tempering we begin by introducing some additional notation. Let $\tilde{N}_0(\psi_*) = N_\phi^0(\psi_*) + 1$ be the number of M_0 SMC stages to obtain a particle swarm that approximates $\pi_0(\theta;\psi_*)$ in (14), including the initial stage, which draws from the prior $p(\theta)$. For the subsequent M_1 model tempering we write the number of stages as $\tilde{N}_1(\psi_*) = N_\phi^1(\psi_*) + 1$, again to emphasize the dependence on ψ_*. We regard $\psi_* = 0$ as M_1 likelihood tempering and adopt the convention that $\tilde{N}_0(0) = 0$.

In the typical VAR and DSGE model applications for which the model tempering procedure is developed, the runtime of the SMC algorithm is predominantly determined by the time it takes to evaluate the likelihood function of the underlying models. Let N_* be the number of likelihood evaluations per SMC stage. It is given by $N_* = N \cdot N_{MH} \cdot N_{blocks}$, where N is the number of particles, N_{MH} is the number of Metropolis-Hastings (MH) steps during the mutation phase, and N_{blocks} is the number of parameter blocks used in each MH step. Moreover, let τ_j be the time it takes to evaluate the likelihood function of model M_j, $j = 0, 1$. Then the total runtime is given by

$$\mathcal{T}(\psi_*, \tau_1, \tau_0) = N_*\left[\tilde{N}_1(\psi_*)\tau_1 + \mathbb{I}\{\psi_* > 0\}(\tilde{N}_1(\psi_*) + \tilde{N}_0(\psi_*))\tau_0\right], \tag{15}$$

where $\mathbb{I}\{x > a\}$ is the indicator function that is equal to one if $x > a$ and equal to zero otherwise. Under likelihood tempering, i.e., $\psi_* = 0$, the likelihood function of M_1 has to be evaluated $N_*\tilde{N}_1(0)$ times and there is no need to evaluate the M_0 likelihood. Under model tempering with $\psi_* > 0$, the likelihood function of M_1 has to be evaluated $\tilde{N}_1(\psi_*)$ times and the likelihood of M_0 needs to be evaluated during the M_0 SMC run and the M_1 SMC run.

Fig. 2: Example: Theoretical Runtime Reductions

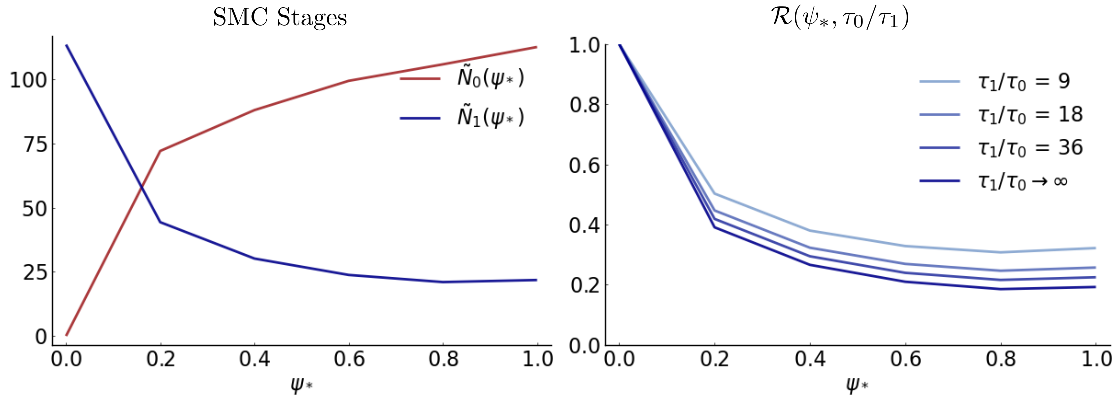

Notes: The left panel shows the functions $\tilde{N}_0(\psi_*)$ and $\tilde{N}_1(\psi_*)$, obtained from DGP 1 of Illustration 2 in Section 4. The right panel depicts $\mathcal{R}(\psi_*, \tau_0/\tau_1)$ in (16).

As mentioned in Section 2.2, we are concerned with the case in which the use of the (tempered) M_0 posterior reduces the number stages for the M_1 SMC and the M_1 likelihood evaluation is substantially faster than the M_0 evaluation:

$$\tilde{N}_1(\psi_*) < \tilde{N}_1(0) \text{ for } \psi_* > 0 \quad \text{and} \quad \tau_0 < \tau_1.$$

In the numerical illustrations in Sections 4 and 5 we report runtimes of model tempering relative to likelihood tempering:[3]

$$\mathcal{R}(\psi_*, \tau_0/\tau_1) = \frac{\mathcal{T}(\psi_*, \tau_1, \tau_0)}{\mathcal{T}(0, \tau_1, \tau_0)} = \frac{\tilde{N}_1(\psi_*)}{\tilde{N}_1(0)} + \mathbb{I}\{\psi_* > 0\} \frac{\tilde{N}_1(\psi_*) + \tilde{N}_0(\psi_*)}{\tilde{N}_1(0)} \frac{\tau_0}{\tau_1}. \tag{16}$$

The first ratio on the right-hand side of (16) captures the effect of reducing the number of M_1 SMC stages needed to reach the target posterior by starting from the tempered M_0 posterior $\pi_0(\theta; \psi_*)$ instead of the prior $p(\theta)$. It does not depend on the relative runtime of the M_1 and M_0 likelihood evaluations. The second term captures the relative costs of having to evaluate the M_0 likelihood function. If $\tilde{N}_1(\psi_*) + \tilde{N}_0(\psi_*) \approx \text{const}$ as a function of ψ_*, then the second term generates a level shift of $\mathcal{R}(\psi_*, \tau_0/\tau_1)$. As the likelihood evaluation of M_0 becomes costless relative to the M_1 likelihood evaluation,

$$\lim_{(\tau_0/\tau_1) \longrightarrow 0} \mathcal{R}(\psi_*, \tau_0/\tau_1) = \frac{\tilde{N}_1(\psi_*)}{\tilde{N}_1(0)}. \tag{17}$$

In the limit, the time it takes to estimate M_0 becomes irrelevant and the reduction is purely driven by the reduction in the number of SMC stages resulting from using an initial distribution that is closer to the target posterior.

In Figure 2 we provide a numerical example for the runtime reduction. In the left panel, we plot functions $\tilde{N}_0(\psi_*)$ and $\tilde{N}_1(\psi_*)$ which are obtained from DGP 1 of the VAR-SV illustration in Section 4. The functions are evaluated at $\psi_* \in \{0.0, 0.2, 0.4, 0.6, 0.8, 1.0\}$. As ψ_* increases, the number of stages used in the M_0 SMC, denoted by $\tilde{N}_0(\psi_*)$, rises, whereas the number stages in the M_1, $\tilde{N}_1(\psi_*)$, falls. The total number of stages required to reach the target posterior stays approximately constant.

The right panel of Figure 2 depicts $\mathcal{R}(\psi_*, \tau_0/\tau_1)$ for various choices of τ_0/τ_1. In this example the most runtime drastic reduction occurs by moving from likelihood tempering to $\psi_* = 0.2$. For $\psi_* \geq 0.6$ the function is essentially flat. In the VAR illustration $\tau_0/\tau_1 = 1/9$. We reduce the likelihood-evaluation ratio

[3] We found that this formula approximates the actual runtime reductions well.

all the way to 0. The figure indicates that the reduction in the ratio creates a modest downward shift of the level because the sum $\tilde{N}_1(\psi_*) + \tilde{N}_0(\psi_*)$ is fairly insensitive to ψ_*.

Thus far, we have provided an *ex post* evaluation of computational gains that relied on knowing how the number of SMC stages depends on ψ through the functions $\tilde{N}_1(\psi_*)$ and $\tilde{N}_0(\psi_*)$. To conduct an *ex ante* assessment, we recommend the researcher first assesses the times τ_j it takes to evaluate the likelihood function of the two models. Moreover, we recommend for several values of ψ_* to compute the variance (across i) of the importance sampling weights

$$\tilde{W}^i(\psi_*) = \frac{\tilde{w}^i(\psi_*)}{\frac{1}{N}\sum_{i=1}^N \tilde{w}^i(\psi_*)}, \quad \tilde{w}^i(\psi_*) = \frac{p(Y|\theta^i, M_1)}{p(Y|\theta^i, M_0)^{\psi_*}}, \tag{18}$$

where the θ^i's are draws from $\pi_0(\theta) \propto p(Y|\theta, M_0)^{\psi_*} p(\theta)$. If there is a $\psi_* > 0$ for which this variance is considerably smaller than for the $\psi_* = 0$ (prior) weights, then there is potential for a substantial runtime reduction. We further explore the relationship between importance sample and runtime reductions in the context of the VAR and DSGE illustrations in Sections 4.3 and 5.3.

3 Illustration 1: Univariate Normal Posteriors

In the first numerical illustration, we consider an environment in which we can directly control the discrepancy between the approximate posterior and the target posterior. We examine the performance of the model tempering approach as a function of the discrepancy between the posteriors. Starting points are "posterior" densities $p(\theta|Y, M_0)$ (approximate) and $p(\theta|Y, M_1)$ (target). We assume that θ is scalar and approximate and target density are both Normal. In particular, we hold the target density fixed at $p(\theta|Y, M_1) \sim N(0, 1)$ and consider a family of approximating densities $p(\theta|Y, M_1) \sim N(\mu, \sigma^2)$, where μ ranges from -3 to 0 in 0.5 increments and σ ranges from 0.2 to 2 in 0.2 increments.

Because in this example we do not construct the posterior density explicitly from a prior distribution and a likelihood function, we let[4]

$$p_n(\theta|Y) = p(\theta|Y, M_1)^{\phi_n} p(\theta|Y, M_0)^{1-\phi_n}$$

and define the incremental weight $\tilde{w}_n^i$ in (3) as

$$\tilde{w}_n^i = \frac{p_n(\theta_{n-1}^i|Y)}{p_{n-1}(\theta_{n-1}^i|Y)}.$$

We run the SMC Algorithm 1 with $N = 1,000$ particles, $\alpha = 0.95$, and use $N_{MH} = 1$ iteration of a single-block random walk Metropolis-Hastings (RWMH) algorithm in the mutation step with $c_0 = 0.5$, targeting an acceptance probability of 0.25. The implementation of the mutation step is described in more detail in the Online Appendix.

Figure 3 illustrates how the particle swarm moves from an approximate posterior to the target posterior, despite very little overlap between the two densities. We overlay the target posterior density, $N(0, 1)$, an approximate density that is used in this example to initialize the algorithm, $N(-3, 0.2)$, and a histogram constructed from the stage n particle swarm. For $n = 0$ (left panel) the particle swarm represents the approximate posterior $p(\theta|Y, M_0)$, and for $n = N_\phi = 71$ (right panel) it represents the target posterior density $p(\theta|Y, M_1)$. In the center panel of the figure we consider the value of $n = 40$ for which the particle swarm represents a weighted geometric mean of the two densities with $\phi_{40} = 0.9$.

In Figure 4 we illustrate the performance of the SMC algorithm across $N_{run} = 100$ runs for the different choices of the approximate posterior. To graphically present the results, we mapped (μ, σ) into a discrepancy measure. In principle one could use the variance of the importance weights defined in (18). However, it turns

[4] This is a slight abuse of notation because $p_n(\theta|Y)$ is not a properly normalized density of θ.

Fig. 3: From Approximate to Target Posterior: $p_n(\theta|Y)$

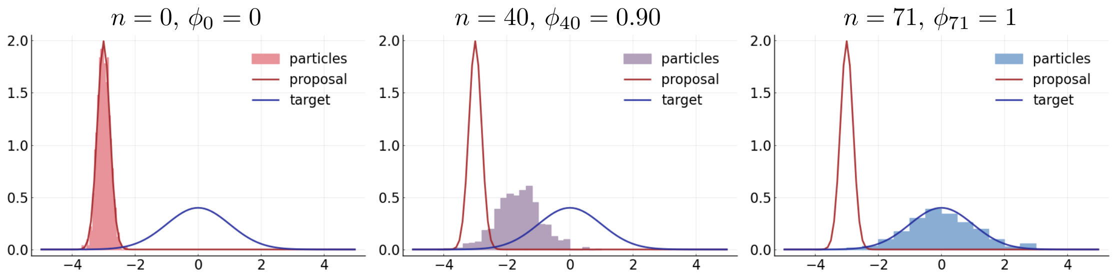

$n = 0,\ \phi_0 = 0$

$n = 40,\ \phi_{40} = 0.90$

$n = 71,\ \phi_{71} = 1$

Notes: Target density is $N(0,1)$ and approximate density is $N(-3,0.2)$.

Fig. 4: Performance of SMC Algorithm

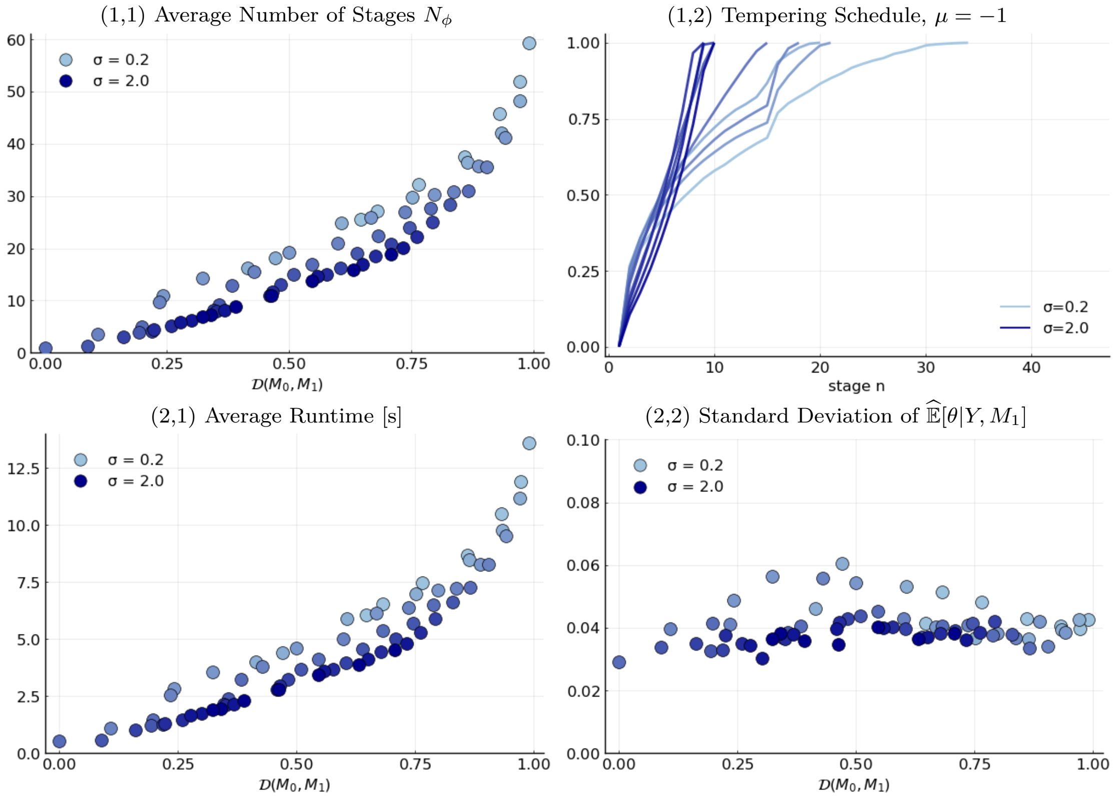

(1,1) Average Number of Stages N_ϕ

(1,2) Tempering Schedule, $\mu = -1$

(2,1) Average Runtime [s]

(2,2) Standard Deviation of $\widehat{\mathbb{E}}[\theta|Y, M_1]$

Notes: Target density is $N(0,1)$ and approximate densities are $N(\mu,\sigma^2)$ where μ ranges from -3 to 0 in 0.5 increments and σ ranges from 0.2 to 2 in 0.2 increments. The statistics panels (1,1) and (2,1) are averaged across $N_{run} = 100$ runs of the SMC algorithm. The standard deviation of the target posterior mean in (2,2) is also computed across multiple runs of the SMC algorithm. In Panel (1,2) we plot the tempering schedules for a single SMC run. Shades of blue indicate different σ values.

out that we consider fairly large discrepancies between M_0 and M_1 for which the population variance of the importance weights is infinite. Thus, in this section we use an alternative discrepancy measure defined as one minus the area under the minimum of the two densities:

$$\mathcal{D}(M_0, M_1) = 1 - \int \min\left\{p(\theta|Y, M_0),\, p(\theta|Y, M_1)\right\} d\theta.$$

By construction $0 \leq \mathcal{D}(M_0, M_1) \leq 1$.

Panel (1,1) shows the average number of stages, N_ϕ, as a function of $\mathcal{D}$. In general, the smaller the discrepancy $\mathcal{D}(M_0, M_1)$, the lower N_ϕ. Because multiple combinations of (μ, σ) can lead to the same $\mathcal{D}(M_0, M_1)$, the graph associates multiple N_ϕ values with particular values of the discrepancy. For the same level of overlap, approximate densities with a larger standard deviation require fewer stages. This observation provides a justification to start the SMC algorithm from a tempered posterior of the approximating model rather than the full posterior.[5]

In Panel (1,2) we depict the tempering schedules for $\mu = -1$ and various values of σ. Because the mean of the approximating density is different from the mean of the target density, increasing the standard deviation σ from 0.2 to 2.0 increases the overlap of the two densities, decreases $\mathcal{D}(M_0, M_1)$, and leads to a steeper tempering schedule. The runtime pattern in Panel (2,1) mirrors the pattern of the average number of stages, because the runtime increases linearly in the number of stages. Finally, we show the standard deviation of the Monte Carlo approximation of $\mathbb{E}[\theta|Y, M_1]$ as a function of $\mathcal{D}(M_0, M_1)$ in Panel (2,2). Here no clear relationship with the discrepancy between approximate and target posterior emerges. Because the tempering schedule is chosen adaptively, the accuracy can be as good for large mismatches as it can be for small discrepancies, but it takes more time in the former case.

We deduce from this example that (i) the speed of the model tempering approach depends on the discrepancy between the approximating and the target density. (ii) Except for the additional runtime, the algorithm still works for fairly large discrepancies between the two densities. (iii) It might be desirable to start from a tempered rather than the full posterior of the approximating model.

4 Illustration 2: A VAR with Stochastic Volatility

This section demonstrates the benefits of model tempering in the context of a VAR with SV. The illustration is based on the VAR analysis in Aruoba et al. (2022), except that we do not include a censored endogenous variable. The VAR model that is used as data generating process (DGP) and then estimated based on simulated data is presented in Section 4.1. The parameterization of the VAR and the tuning of the SMC algorithm are summarized in Section 4.2. The numerical results are discussed in Section 4.3.

4.1 VAR Specification

Model M_1 is taken to be a bivariate VAR(1) with stochastic volatility:

$$y_t = \Phi_1 y_{t-1} + \Phi_c + \mathrm{chol}(\Sigma)\varepsilon_t, \quad \varepsilon_t \sim N(0, D_t), \quad D_t = \mathrm{diag}(d_t), \tag{19}$$

where Σ is a symmetric positive definite matrix and $\mathrm{chol}(\cdot)$ is the lower-triangular Cholesky factor. Let $d_t = [d_{1,t}, d_{2,t}]'$ and assume that its elements evolve according to

$$\ln d_{it} = \rho_i \ln d_{it-1} + \xi_i \eta_t^i, \quad \eta_t^i \sim N(0, 1), \quad i = 1, 2. \tag{20}$$

The presence of stochastic volatility renders this model nonlinear. However, the conditional linearity makes the likelihood evaluation relatively straightforward. We use a Bootstrap Particle Filter (BSPF) with $M_{bspf} = 100$ particles, as outlined in the Online Appendix, to sequentially integrate out the latent volatility states. The BSPF likelihood evaluation can be conveniently integrated into the SMC sampler described in Algorithm 1.[6] Moreover, this computational strategy is very similar to a Bayesian estimation approach widely-used for the estimation of nonlinear DSGE models. We will use the BSPF also in Section 5.

[5] This observation is related to the well-known importance sampling result that the proposal density should have fatter tails than the target density; see, e.g., Geweke (1989).

[6] The use of a particle filter to evaluate the likelihood in the SMC posterior sampler results in a SMC^2 algorithm, as discussed in Chopin et al. (2013).

Tab. 1: Parameterizations of the SV Processes

	ρ_1	ρ_2	ξ_1	ξ_2
DGP 1	**0.50**	**0.90**	**0.20**	**0.20**
DGP 2	**0.20**	**0.60**	**0.80**	**0.90**
DGP 3	**0.50**	**0.90**	**0.80**	**0.90**

The approximating model M_0 is identical to M_1 except that it ignores stochastic volatility. It is given by the homoskedastic VAR

$$y_t = \Phi_1 y_{t-1} + \Phi_c + u_t, \quad u_t \sim N(0, \Sigma). \tag{21}$$

In other words, M_0 is obtained by setting $\xi_i = 0 \; \forall \; i$. This restriction renders (ρ_i, ξ_i) non-identified. One obtains the standard analytical expression for the likelihood of a VAR, which as a result can be evaluated instantaneously. Thus, one important condition that makes model tempering attractive is satisfied: the evaluation of the likelihood function for the approximating model is considerably faster than the evaluation of the target model's likelihood.

We use a version of the Minnesota prior for (Φ_1, Φ_c, Σ). The (marginal) prior for each ρ_i is a Uniform distribution, while that for ξ_i is an inverse Gamma distribution. Further details on the prior are provided in the Online Appendix. The prior specification is the same for all DGP parameterizations.

4.2 Parameterization of DGP and Tuning of Algorithm

Estimation is conducted on $T = 100$ observations simulated from model M_1. We use the following parameterization for (Φ_1, Φ_c, Σ):

$$\Phi_1 = \begin{bmatrix} 0.6 & 0.3 \\ 0.0 & 0.4 \end{bmatrix}, \quad \Phi_c = \begin{bmatrix} 0.0 \\ 0.0 \end{bmatrix}, \quad \Sigma = \begin{bmatrix} 1.0 & 0.0 \\ 0.7 & 1.0 \end{bmatrix} \cdot \begin{bmatrix} 1.0 & 0.7 \\ 0.0 & 1.0 \end{bmatrix} = \begin{bmatrix} 1.00 & 0.70 \\ 0.70 & 1.49 \end{bmatrix}.$$

The closeness of the posteriors under the target model (VAR with SV) and the approximating model (homoskedastic VAR) depends on the parameterization of the stochastic volatility processes. We consider three different parameterizations which are summarized in Table 1. Under DGP 1 (baseline) the standard deviations of the log volatility innovations are relatively small. This implies that the $\ln d_{it}$s only exhibit modest time variation and the homoskedastic specification provides a good approximation. Under DGP 2 the volatility innovations have larger standard deviations but the log volatility processes are less persistent, implying large yet short-lived swings in volatility. Finally, DGP 3 combines the baseline values for ρ_i with the large values of ξ_i also considered under DGP 2, implying the largest distance between the approximating model and the target model. This is confirmed in Figure 5. The panels in the top row show the volatility paths, d_{1t} and d_{2t}, and the bottom row illustrates the resulting discrepancy between the M_0 and M_1 posteriors, using the parameter $\Phi_{1,21}$ as an example.

We use an adaptive tempering schedule with $\alpha = 0.95$, as described in Section 2.3, to ensure that the number of SMC stages and hence the computational time adjust endogenously to the distance between the proposal and the target density. We initialize the SMC algorithm based on the following set of tempered M_0 posteriors:

$$\pi_0(\theta) \propto p(Y|\theta, M_0)^{\psi_*} p(\theta), \quad \psi_* \in \{0.0, 0.2, 0.4, 0.6, 0.8, 1.0\},$$

where $\psi_* = 0$ corresponds to likelihood tempering, i.e., estimation of M_1 without using information from model M_0. Higher values for ψ_* increasingly tilt the proposal density away from the prior distribution towards the posterior under the proxy model M_0. For $\phi_* = 1$, the proposal density coincides with the posterior under M_0. This is illustrated in Figure 6 which shows along with the M_1 target posterior the

Fig. 5: Stochastic Volatility Paths and M_0 vs. M_1 Posteriors

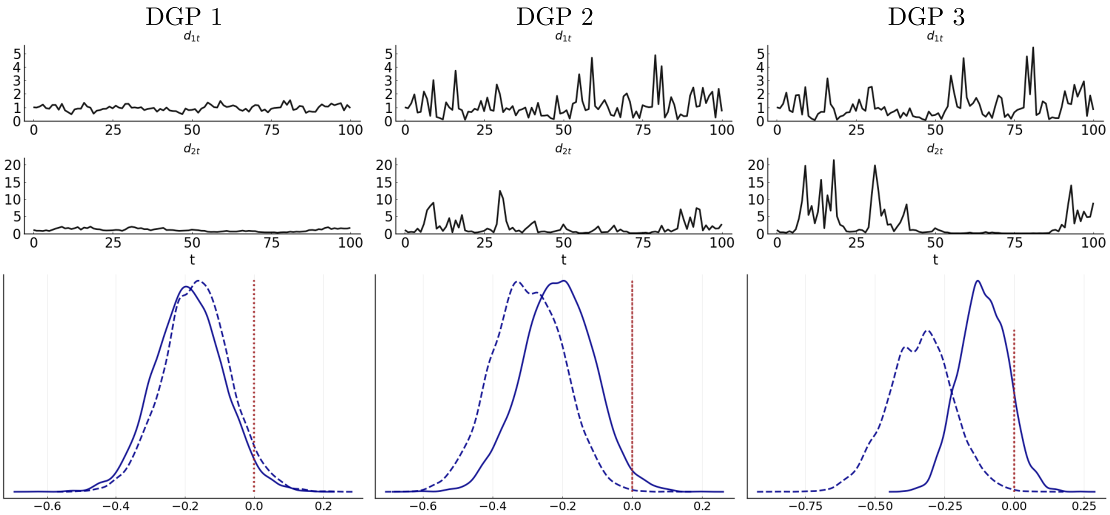

Notes: Top row: simulated volatility paths d_{1t}. Middle row: simulated volatility paths d_{2t}. Bottom row: M_0 (dashed black) versus M_1 (solid blue) posterior densities for $\Phi_{1,21}$. Dotted vertical line indicates true value.

Fig. 6: Approximate Distributions for $\Phi_{1,21}$, DGP 2

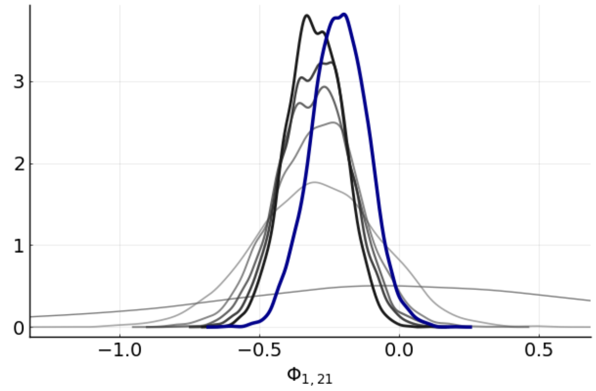

Notes: The approximating posterior densities obtained from the tempered M_0 likelihood function for $\psi_* \in \{0.0, 0.2, 0.4, 0.6, 0.8, 1.0\}$ are plotted in shades (the larger ψ_* the darker) of gray. The M_1 posterior is depicted in blue.

sequence of approximating posterior distributions for $\Phi_{1,21}$ under DGP 2 obtained from the ψ_*-tempered M_0 likelihood function.

The number of particles in the SMC sampler is set to $N = 500$. For each DGP and $\pi_0(\theta)$ we run the SMC algorithm $N_{run} = 200$ times. We subsequently report averages across the N_{run} runs and assess the variance of the Monte Carlo approximations across runs.

4.3 Results

The left panel of Figure 7 plots average (across multiple SMC runs) Monte Carlo approximates of the log MDD of model M_1, $\ln p(Y|M_1)$, under DGP 1 as a function of ψ_*, i.e. as a function of the degree of model

Fig. 7: Log MDD and Precision

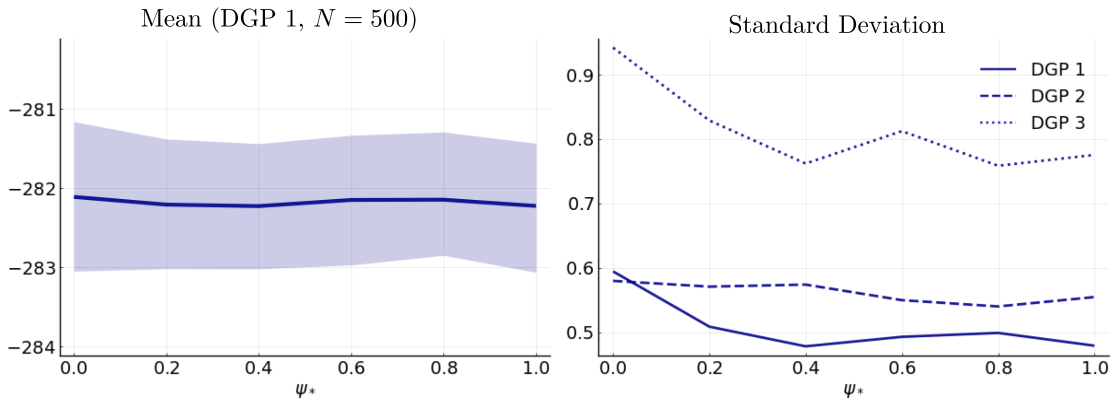

Notes: The left panel depicts the mean and 90% credible bands based on $N_{run} = 200$ runs for DGP 1 with $N = 500$ particles. The right panel shows the standard deviation of log MDD across the runs for all considered setups.

Fig. 8: VAR-SV: Computational Times and Initial Variance of Particle Weights

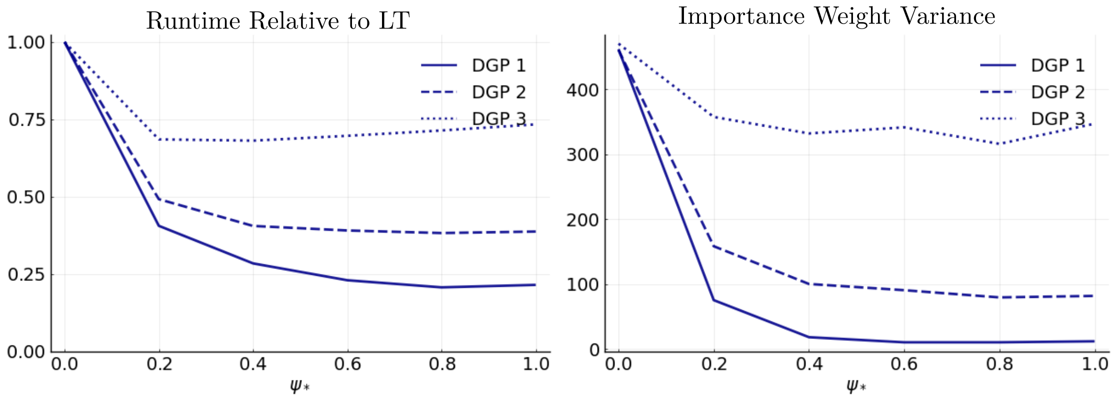

Notes: The left panel plots the computational time relative to LT ($\phi_{N_\phi}(M_0) = 0$) for the three DGPs (all with $N = 500$). The right panel depicts the variance of particle weights $\tilde{W}^i(\psi_*)$ defined in (18). In both panels we depict averages across the $N_{run} = 200$ runs.

tempering used in the construction of $\pi_0(\theta;\psi_*)$. The flat line confirms that the Monte Carlo approximations are the same regardless of $\pi_0(\theta;\psi_*)$, as we are numerically approximating the same object regardless of ψ_*. The shaded area is a 95% credible band for the log MDD. Figure A-4 in the Online Appendix confirms that the Monte Carlo approximations for posterior mean, variance, 5th and 95th percentiles of the VAR parameters are also invariant to ψ_*. Moreover, the result holds not just under DGP 1, but also the other two DGPs (not shown in the figures).

The right panel of Figure 7 shows the standard deviation of the Monte Carlo approximation of the log MDD as a function of ψ_* for the three different DGPs. For DGP 1 and DGP 3 the standard deviations are weakly decreasing in ψ. The biggest drop occurs between $\psi_* = 0$ and $\psi_* = 0.2$. For DGP 2 the profile is approximately flat, that is, based on the discrepancy between approximating density and target density, the algorithm adjusts the number of stages to keep the accuracy of the Monte Carlo approximation approximately constant.

We now proceed by examining how ψ_* affects the runtime of the SMC algorithm. The main result is presented in Figure 8. The left panel compares the runtime profiles (normalized by the LT runtime) across the three DGPs. Incorporating information from model M_0 in the construction of the proposal density drastically reduces the runtime. The ratio of likelihood evaluation times for M_0 and M_1 is $\tau_0/\tau_1 = 9.14$. For DGP 1 the runtime monotonically decreases as the proposal is increasingly tilted towards the posterior of the approximate model M_0, with the largest reduction of close to 80% obtained for $\psi_* \in \{0.6, 0.8, 1.0\}$. The runtime reduction is largest for DGP 1, followed by DGP 2, while DGP 3 is associated with the smallest reduction.

The steepest decrease in runtime occurs at $\psi_* = 0.2$, which means that incorporating just a bit of information from the approximate model M_0 when constructing the proposal density for the posterior of model M_1 goes a long way in reducing the runtime. Adding more information helps little at best and might be even counterproductive, as is the case for DGP 3. In principle, for an even larger distance between the posteriors under the two models, it is conceivable that there is no runtime reduction at all. In this case, the second condition stated in Section 2.2 would be violated.

The runtime benefits of model tempering decrease with the distance between the posteriors under the target model M_1 and the approximate model M_0.[7] In our VAR application, this distance increases with the nonlinearities generated by the SV specification, which are strongest for DGP 3. This distance is visualized in Figures A-1, A-2 and A-3 in the Online Appendix. While for DGP 1 all marginal posteriors align very well for the two models, for DGP 3 there are some parameters for which there is little overlap of probability mass between the two distributions.

We discussed in Section 2.4 that this distance could be assessed *ex ante*, without having completed the SMC run for M_1, by computing the variance of the importance sampling weights defined in (18). The variances as a function of ψ_* for the three DGPs are depicted in the right panel of Figure 8. The variance profiles look very similar to the runtime profiles in the left panel. For $\psi_* = 0$ the variance is approximately equal to the number of particles minus one, $N - 1$, which means that one of the particles has weight N and the remaining particles have weight zero. For $\psi_* = 0.2$ the variance is considerably lower: it is 75 for DGP 1 and 357 for DGP 3.

To summarize, in this VAR-SV application model tempering is able to reduce the relative runtime by between 27% (DGP 3) and 79% (DGP 1) and increase the precision of Monte Carlo approximations (DGP 1 and 3).

5 Illustration 3: Two Nonlinear DSGE Models

Finally, we consider the estimation of two nonlinear DSGE models, which are computationally demanding for two reasons: first, the model needs to be solved and, second, the evaluation of the likelihood function requires a nonlinear filter. For the latter task, we will use a particle filter similar to the one used to estimate the VAR with SV in Section 4. Most of this section focuses on a small RBC model with asymmetric quadratic capital adjustment costs. The adjustment cost parameters let us control the degree of nonlinearity. The model economy is described in Section 5.1, the configuration of the simulation experiment is summarized in Section 5.2, and the simulation results are presented in Section 5.3. In Section 5.4 we repeat the analysis with a larger New Keynesian DSGE model that features asymmetric wage and price rigidities of Aruoba et al. (2017), henceforth ABS.

[7] The runtime for DGP 3 also exhibits the most variation across multiple runs; see Figure A-5 in the Online Appendix. Depending on the run, there could be many or only very few particles in the small area to which both posteriors assign some positive probability mass.

5.1 Model Specification

The model economy consists of a representative household and a representative firm. The household consumes C, supplies labor in the amount of L, and owns the capital stock K. The firm hires labor and rents capital to produce a single good that can be used for consumption and investment. The model dynamics can be described as the solution to the following social planner problem:

$$\begin{aligned} V(K,S) \quad &= \quad \max_{C,L,K'} \frac{C^{1-\tau}-1}{1-\tau} - B\frac{L^{1+1/\nu}}{1+1/\nu} + \beta\mathbb{E}_{S'|S}[V(K',S')] \\ \text{s.t.} \quad & C + I + K\Phi(K'/K) = Y, \\ & Y = ZK^{\alpha}L^{1-\alpha}, \\ & I = K' - (1-\delta)K. \end{aligned} \tag{22}$$

Households derive utility from consumption and disutility from labor. The parameter β is the discount factor, τ determines the risk aversion, and ν is the Frisch labor supply elasticity. The parameter α is the capital share parameter, and δ the depreciation rate. Total factor productivity Z and the preference process B evolve exogenously according to AR(1) laws of motion:

$$\begin{aligned} Z \quad &= Z_* e^{\hat{z}}, \quad \hat{z}' = \rho_z \hat{z} + \sigma_z \varepsilon_z', \\ B \quad &= B_* e^{\hat{b}}, \quad \hat{b}' = \rho_b \hat{b} + \sigma_b \varepsilon_b' \ . \end{aligned} \tag{23}$$

Thus, ε_z' can be thought of as a supply and ε_x' as a demand shock. Here we adopt the convention that for a variable X, X_* denotes the steady state and $\hat{x}$ denote log deviations from the steady state.

For the adjustment cost function we use a linex function which is asymmetric:

$$\Phi(K'/K) = \phi_1 \left(\frac{\exp(-\phi_2(K'/K-1)) + \phi_2(K'/K-1) - 1}{\phi_2^2} \right). \tag{24}$$

The parameter ϕ_1 controls the overall level of adjustment costs and ϕ_2 determines the asymmetry. Notice that as $\phi_2 \longrightarrow 0$ the adjustment costs become quadratic around the replacement investment level at which $K'/K = 1$. If $\phi_2 > 0$, then it is more costly to reduce the capital stock than it is to augment the capital stock.

Model M_1 refers to a nonlinear solution of the RBC growth model, obtained using a second-order perturbation around the steady state. The approximate model M_0 is obtained by conducting a first-order linearization. The models are estimated based on observations for output, investment, and hours worked. We denote the observed variables by an o-superscript. The measurement equations, now with t subscripts, take the form:

$$\begin{aligned} \ln Y_t^o \quad &= \quad \ln Y_t + \eta_{Y,t}, \quad \eta_{Y,t} \sim N(0,\sigma_Y^2), \\ \ln I_t^o \quad &= \quad \ln I_t + \eta_{I,t}, \quad \eta_{I,t} \sim N(0,\sigma_I^2), \\ \ln L_t^o \quad &= \quad \ln L_t + \eta_{L,t}, \quad \eta_{L,t} \sim N(0,\sigma_L^2), \end{aligned} \tag{25}$$

where $\ln Y_t$, $\ln I_t$, and $\ln L_t$ are the model-implied series and the η_ts are measurement errors. The measurement errors facilitate the use of a particle filter in combination with the nonlinear DSGE model solution. Moreover, they help to overcome the singularity problem generated by fitting a DSGE model with two shocks to three observables. We include the measurement errors in both data generation and estimation and fix their standard deviations such that the variance of the measurement error is approximately 5% of the variation of the series $\ln Y_t$, $\ln I_t$, and $\ln L_t$, respectively.[8]

[8] The values that we use are $\sigma_Y = .006$, $\sigma_I = .004$, and $\sigma_L = .004$.

Tab. 2: DGP and Prior

	True			**Prior Distribution**		
	Value	**Density**	**P(1)**	**P(2)**	**HPD Low**	**HPD High**
r	**3.00**			**fixed at 3.00**		
δ	**0.08**			**fixed at 0.08**		
τ	**2.00**	$\mathcal{G}$	**1.00**	**1.00**	**.0005**	**2.27**
ν	**1.00**	$\mathcal{G}$	**0.50**	**0.30**	**0.07**	**0.87**
α	**0.35**	$\mathcal{B}$	**0.35**	**0.05**	**0.27**	**0.43**
ϕ_1	**50.0**	$\mathcal{G}$	**30.0**	**15.0**	**8.47**	**50.8**
ϕ_2	**200**	$\mathcal{N}$	**0**	**75.0**	**-123**	**116**
ρ_z	**0.95**	$\mathcal{B}$	**0.6**	**0.15**	**0.35**	**0.80**
ρ_b	**0.90**	$\mathcal{B}$	**0.6**	**0.15**	**0.38**	**0.82**
$100\sigma_z$	**2.00**	$\mathcal{IG}$	**1.50**	**5.00**	**0.45**	**2.27**
$100\sigma_b$	**1.60**	$\mathcal{IG}$	**1.50**	**5.00**	**0.53**	**2.35**

Notes: We set $Y_* = L_* = 1$ and we define $r = 400(1/\beta - 1)$. $\mathcal{G}$ is Gamma distribution; $\mathcal{B}$ is Beta distribution; $\mathcal{IG}$ is Inverse Gamma distribution; and $\mathcal{N}$ is Normal distribution, and $\mathcal{U}$ is Uniform distribution. P(1) and P(2) are mean and standard deviations for $\mathcal{B}$, $\mathcal{G}$, and $\mathcal{N}$ distributions. The $\mathcal{U}$ distribution is parameterized in terms of lower and upper bound. The $\mathcal{IG}$ distribution is parameterized as scaled inverse χ^2 distribution with density $p(\sigma^2|s^2,\nu) \propto (\sigma^2)^{-\nu/2-1}\exp[-\nu s^2/(2\sigma^2)]$, where P(1) is $\sqrt{s^2}$ and P(2) is ν. The density of σ is obtained by the change of variables $\sigma = \sqrt{\sigma^2}$. HPD(Low,High) refers to the boundaries of 90% highest prior density intervals.

5.2 Model Parameterization and Tuning of Algorithm

To facilitate the estimation, we reparameterize the model as follows. First, we express the discount factor β as a function of an annualized real interest rate (in percentages) $r = 400(1/\beta - 1)$. Second, instead of parameterizing the model in terms of steady states of the exogenous processes (Z_*, B_*), we use the steady states of output and labor, (Y_*, L_*), which we set equal to one for both data generation and estimation. Because our observations $\ln Y_t^o$, $\ln I_t^o$, and $\ln L_t^o$ do not contain direct information on the steady state interest rate and the amount of investment necessary to replace depreciating capital stock, we fix r and δ at their true values. We collect the parameters that are being estimated in the vector θ:

$$\theta = [\tau, \nu, \alpha, \phi_1, \phi_2, \rho_z, \rho_b, 100\sigma_z, 100\sigma_b]'.$$

As in Section 4, the estimation is conducted using data simulated from model M_1. The parameterization of the DGP is summarized in Table 2. Most of the parameter values are similar to values commonly found in the DSGE model literature, except that we scale up the shock standard deviations and use fairly large asymmetric adjustment costs by setting $\phi_1 = 50$ and $\phi_2 = 200$. We plot simulated sample paths in the Online Appendix. The length of the estimation sample is $T = 80$. The remaining columns of Table 2 describe the prior distribution for the Bayesian estimation.

In the SMC algorithm we use $N = 1,000$ particles to represent the distribution of θ, $N_{MH} = 2$ Metropolis-Hastings steps in the mutation, and an adaptive tempering schedule with $\alpha = 0.95$. While the likelihood function associated with M_0 can be evaluated with the Kalman filter, a nonlinear filter is required to compute the likelihood function of M_1. We use the same BSPF that was used in Section 4 for the VAR estimation with $M_{bspf} = 2,000$ particles.

5.3 Results

As before, we consider $\psi_* \in \{0.0, 0.2, 0.4, 0.6, 0.8, 1.0\}$, where $\psi_* = 0$ corresponds to M_1 likelihood tempering. The relative time it takes to evaluate the M_0 and M_1 likelihood functions is $\tau_0/\tau_1 \approx 1/109$. This ratio depends on the number of particles M_{bspf} used in the BSPF. Doubling M_{bspf} would approximately double

Fig. 9: Results from the RBC Model

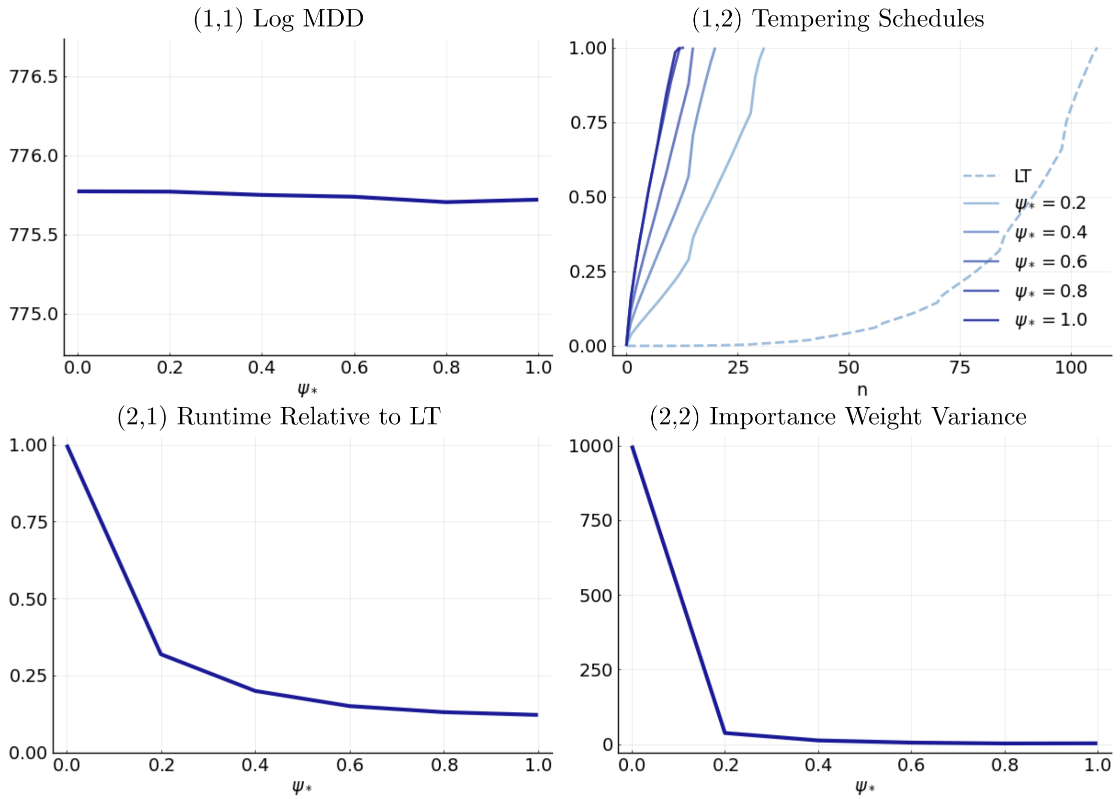

Notes: Results are based on a single run ($N_{run} = 1$). Panel (1,1) plots the log MDD as a function of the tempering parameter ψ_*, panel (1,2) shows the tempering schedules for different ψ_*, panel (2,1) plots the computational time relative to LT ($\phi_{N_\phi}(M_0) = 0$), and panel (2,2) depicts the variance of particle weights $\tilde{W}^i(\psi_*)$ defined in (18).

τ_1 and cut the ratio in half. The numerical results from a single $N_{run} = 1$ run of the model tempering SMC algorithm for the various values of ψ_* are presented in Figure 9. The top left (1,1) panel shows the log MDD approximation, which is approximately constant as a function of ψ_*. This plot confirms that regardless of ψ_* the SMC algorithm delivers the same approximations of the posterior distribution.

The tempering schedules are plotted in Panel (1,2). Starting from a (tempered) M_0 posterior drastically reduces the number of stages needed to reach the target posterior. This is consistent with the information provided by the importance weight variance in Panel (2,2). Reweighting draws from the prior $p(\theta)$ ($\psi_* = 0$) to target the M_1 posterior would lead to a degenerate distribution of weights, whereby the weight of one draw is equal to one and all other weights are equal to zero. Starting with draws from the $\psi_* = 0.2$ tempered M_0 posterior reduces the importance weight variance from $N - 1 = 999$ to 37. Raising ψ_* toward one, lowers the variance further.

Panel (2,1) depicts the runtime of the model-tempered SMC relative to the M_1 likelihood-tempered SMC. The biggest drop, from 1.0 to 0.3 occurs by raising ψ_* from 0.0 to 0.2. Subsequent gains are smaller and the curve essentially turns flat from 0.8 onwards, converging to 0.12. In terms of absolute runtimes, on a Windows workstation with Intel(R) Xeon(R) CPU E5-2687 at 3.10GHz using 8 out of 10 cores model tempering with $\psi_* = 1$ reduces the runtime of our JULIA code from 655 to 80 minutes. In the Online Appendix we plot the target and approximate (marginal) posterior densities for the DSGE model parameters. Despite the large ϕ_1 and ϕ_2 values, the nonlinearity generated by the DSGE model is not particularly strong and M_0 and M_1 posterior distributions are quite similar. Thus, when starting from $\psi_* = 0.8$ or

$\psi_* = 1$ only minimal adjustments are required to turn the M_0 posterior draws into M_1 posterior draws which leads to substantial computational gains.

5.4 A New Keynesian DSGE Model

As a second DSGE model illustration we consider a New Keynesian DSGE model in which asymmetric price and wage adjustment costs generate nonlinear dynamics. The model is taken from ABS. It consists of final goods producing firms, a continuum of intermediate goods producing firms, a representative household, and monetary and fiscal authorities. The model replaces Rotemberg-style quadratic adjustment cost functions for wages and prices by linex adjustment cost functions, which can capture downward (as well as upward) nominal rigidities. The model abstracts from capital accumulation. We simulate a sample of length $T = 92$ from the DSGE model using the posterior mean estimates for the period 1984:Q1-2007:Q4 reported in Table 3 of ABS and conduct Bayesian estimation based on the prior distribution summarized in the same Table.

As before, we use $N = 1,000$ particles, set $\alpha = 0.95$, and $N_{MH} = 2$ (no blocking). The likelihood function of the nonlinear version of the DSGE model is evaluated with the BSPF using $M_{bspf} = 25,000$. We increase the number of particles for the filter to ensure that the likelihood approximation is sufficiently accurate to be usable for parameter estimation. We start the model tempering from the full posterior, setting $\psi_* = 1$. In this environment, the relative time to evaluate the likelihood functions drops to $\tau_0/\tau_1 \approx .00004$. This reflects the increases number of particles in the BSPF as well as more costly BSPF runs due to a larger-dimensional state space in this model. Conducting a single run of the algorithm we find that model tempering instead of likelihood tempering reduces the runtime by approximately 80%, which is similar to the reduction in the RBC model application. Because τ_0/τ_1 is close to zero, we deduce from (17) that the runtime reduction is driven by the reduction in the number of stages achieved by model tempering relative to likelihood tempering, $\tilde{N}(1)/\tilde{N}(0)$.

6 Conclusion

The implementation of posterior samplers for Bayesian inference often requires the explicit evaluation of likelihood functions. Likelihood calculations for macroeconometric models can be computationally demanding, because it may take a long time to solve the underlying structural model or it may be time-consuming to integrate out latent state variables. In this paper we documented how an SMC algorithm with model tempering can speed up posterior sampling for a VAR with stochastic volatility and a nonlinear DSGE model. The method is suitable for applications in which the likelihood evaluation for the target model is computationally costly and there is an approximating model for which the likelihood evaluation is fast and that generates a posterior that is not too different from the posterior of the target model.

Acknowledgment: We thank Marco Del Negro, David Childers, and seminar and conference participants at Penn, the 2021 Conference of Swiss Economists Abroad, the 2022 Barcelona GSE Summer Forum, the 2022 Annual Conference of the IAAE in London, the 2022 ESOBE Meetings in Salzburg, and the 2022 FRB Philadelphia Conference on Frontiers in Machine Learning and Economics for helpful comments and discussions.

Funding: Schorfheide gratefully acknowledges financial support from the National Science Foundation under Grant SES 1851634.

References

Acharya, S., W. Chen, M. Del Negro, K. Dogra, E. Matlin, and R. Sarfati (2021): "Estimating HANK: Macro Time Series and Micro Moments," *Working Paper, Federal Reserve Bank of New York*.

Aruoba, B., L. Bocola, and F. Schorfheide (2017): "Assessing DSGE Model Nonlinearities," *Journal of Economic Dynamics & Control*, 83, 34–54.

Aruoba, B., M. Mlikota, F. Schorfheide, and S. Villalvazo (2022): "SVARs with Occasionally-Binding Constraints," *Journal of Econometrics*, forthcoming.

Bon, J. J., A. Lee, and C. Drovandi (2021): "Accelerating Sequential Monte Carlo with Surrogate Likelihoods," *Statistics and Computing*, 31, 1–26.

Cai, M., M. Del Negro, E. Herbst, E. Matlin, R. Sarfati, and F. Schorfheide (2021): "Online Estimation of DSGE Models," *Econometric Journal*, 24, C33–58.

Chopin, N. (2002): "A Sequential Particle Filter for Static Models," *Biometrika*, 89, 539–551.

Chopin, N., P. E. Jacob, and O. Papaspiliopoulos (2013): "SMC^2: an efficient algorithm for sequential analysis of state space models," *Journal of the Royal Statistical Society: Series B (Statistical Methodology)*, 75, 397–426.

Christen, A. J. and C. Fox (2005): "Markov Chain Monte Carlo Using an Approximation," *Journal of Computational and Graphical Statistics*, 14, 795–810.

Creal, D. (2007): "Sequential Monte Carlo Samplers for Bayesian DSGE Models," *Manuscript, University Chicago Booth*.

Dai, C., J. Heng, P. E. Jacob, and N. Whiteley (2022): "An Invitation to Sequential Monte Carlo Samplers," *Journal of the American Statistical Association*, 117, 1587–1600.

Del Moral, P., A. Doucet, and A. Jasra (2012): "An Adaptive Sequential Monte Carlo Method for Approximate Bayesian Computation," *Statistical Computing*, 22, 1009–1020.

Del Negro, M. and F. Schorfheide (2012): "DSGE Model Based Forecasting," in *Handbook of Economic Forecasting*, ed. by G. Elliot and A. Timmermann, Elsevier, vol. 2, forthcoming.

Doppelt, R. and K. O'Hara (2020): "Bayesian Estimation of Fractionally Integrated Vector Autoregressions and an Application to Identified Technology Shocks," *Working Paper, Penn State University*.

Durham, G. and J. Geweke (2014): "Adaptive Sequential Posterior Simulators for Massively Parallel Computing Environments," in *Advances in Econometrics*, ed. by I. Jeliazkov and D. Poirier, Emerald Group Publishing Limited, West Yorkshire, vol. 34, chap. 6, 1–44.

Geweke, J. (1989): "Bayesian Inference in Econometrics Models Using Monte Carlo Integration," *Econometrica*, 57, 1317–1339.

Geweke, J. and B. Frischknecht (2014): "Exact Optimization By Means of Sequentially Adaptive Bayesian Learning," *Manuscript, University of Iowa*.

Gordon, N., D. Salmond, and A. F. Smith (1993): "Novel Approach to Nonlinear/Non-Gaussian Bayesian State Estimation," *Radar and Signal Processing, IEE Proceedings F*, 140, 107–113.

Herbst, E. and F. Schorfheide (2014): "Sequential Monte Carlo Sampling for DSGE Models," *Journal of Applied Econometrics*, 29, 1073–1098.

——— (2015): *Bayesian Estimation of DSGE Models*, Princeton University Press.

——— (2019): "Tempered Particle Filtering," *Journal of Econometrics*, 210, 26–44.

Hoogerheide, L., A. Opschoor, and H. van Dijk (2012): "A Class of Adaptive Importance Sampling Weighted EM Algorithms for Efficient and Robust Posterior and Predictive Simulation," *Journal of Econometrics*, 171, 101–120.

Jasra, A., D. A. Stephens, A. Doucet, and T. Tsagaris (2011): "Inference for Levy-Driven Stochastic Volatility Models via Adaptive Sequential Monte Carlo," *Scandinavian Journal of Statistics*, 38, 1–22.

Kim, S., N. Shephard, and S. Chib (1998): "Stochastic Volatility: Likelihood Inference and Comparison with ARCH Models," *Review of Economic Studies*, 65, 361–393.

Kloek, T. and H. K. van Dijk (1978): "Bayesian Estimates of Equation System Parameters: An Application of Integration by Monte Carlo," *Econometrica*, 46, 1–19.

Liu, J. S. (2001): *Monte Carlo Strategies in Scientific Computing*, Springer, New York.

Mathews, J. and S. C. Schmidler (2022): "Finite Sample Complexity of Sequential Mote Carlo Estimators on Multimodal Target Distributions," *arXiv Working Paper 2208.06672*.

Schäfer, C. and N. Chopin (2013): "Sequential Monte Carlo on Large Binary Sampling Spaces," *Statistical Computing*, 23, 163–184.

Schmitt-Grohé, S. and M. Uribe (2004): "Solving Dynamic General Equilibrium Models Using a Second-Order Approximation to the Policy Function," *Journal of Economic Dynamics and Control*, 28, 755–775.

Smets, F. and R. Wouters (2007): "Shocks and Frictions in US Business Cycles: A Bayesian DSGE Approach," *American Economic Review*, 97, 586–606.

Smith, M. (2011): "Estimating Nonlinear Economics Models Using Surrogate Transitions," *Working Paper, Federal Reserve Board*.

Zhou, Y., A. M. Johansen, and J. A. Aston (2015): “Towards Automatic Model Comparison: An Adaptive Sequential Monte Carlo Approach,” *arXiv Working Paper*, 1303.3123v2.

Online Appendix: Sequential Monte Carlo with Model Tempering

Marko Mlikota and Frank Schorfheide

This Appendix consists of the following sections:
A. Computational Details
B. Illustration 2: VAR with Stochastic Volatility
C. Illustration 3: A Nonlinear DSGE Model

A Computational Details

The presentations of the mutation algorithm in Section A.1 and the BSPF in in Section A.2 are based on Herbst and Schorfheide (2015).

A.1 SMC Particle Mutation

Algorithm 2 (Particle Mutation).
In Step 2(c) in iteration n of Algorithm 1:

1. *Compute an importance sampling approximation* $\tilde{\Sigma}_n$ *of* $\mathbb{V}_{\pi_n}[\theta]$ *based on the particles* $\{\theta^i_{n-1}, \tilde{W}^i_n\}_{i=1}^N$.
2. *Compute the average empirical rejection rate* $\hat{R}_{n-1}(\hat{\zeta}_{n-1})$, *based on the Mutation step in iteration* $n-1$. *The average is computed across the* N_{blocks} *blocks.*
3. *Let* $\hat{c}_1 = c^*$ *and for* $n > 2$ *adjust the scaling factor according to*
$$\hat{c}_n = \hat{c}_{n-1} f\big(1 - \hat{R}_{n-1}(\hat{\zeta}_{n-1})\big),$$
where
$$f(x) = 0.95 + 0.10\frac{e^{16(x-0.25)}}{1+e^{16(x-0.25)}}.$$
4. *Define* $\hat{\zeta}_n = \big[\hat{c}_n, vech(\tilde{\Sigma}_n)'\big]'$.
5. *For each particle i, run* N_{MH} *steps of a Random Walk Metropolis-Hastings Algorithm using the proposal density*
$$\vartheta^{i,m}_n|\hat{\zeta}_n \sim N\bigg(\theta^{i,m-1}_n, \hat{c}^2_n\tilde{\Sigma}_n\bigg). \tag{A.1}$$

A.2 (Particle) Filtering

We use a bootstrap particle filter (BSPF) to approximate the likelihood function in the model with stochastic volatility. In the description of the filter we denote the latent state by s_t.

Algorithm 3 (Bootstrap Particle Filter).

1. **Initialization.** *Draw the initial particles from the distribution* $s^j_0 \overset{iid}{\sim} p(s_0|\theta)$ *and set* $W^j_0 = 1$, $j = 1,\dots,M$.
2. **Recursion.** *For* $t = 1,\dots,T$*:*
   (a) **Forecasting** s_t**.** *Draw* $\tilde{s}^j_t$ *from the state-transition density* $p(\tilde{s}_t|s^j_{t-1},\theta)$.
   (b) **Forecasting** y_t**.** *Define the incremental weights*
$$\tilde{w}^j_t = p(y_t|\tilde{s}^j_t, Y_{1:t-1},\theta) \tag{A.2}$$
The predictive density $p(y_t|Y_{1:t-1},\theta)$ *can be approximated by*
$$\hat{p}(y_t|Y_{1:t-1},\theta) = \frac{1}{M}\sum_{j=1}^M \tilde{w}^j_t W^j_{t-1}. \tag{A.3}$$

(c) *Define the normalized weights*

$$\tilde{W}_t^j = \tilde{w}_t^j W_{t-1}^j \bigg/ \frac{1}{M}\sum_{j=1}^{M} \tilde{w}_t^j W_{t-1}^j. \tag{A.4}$$

(d) **Selection.** *Resample the particles, for instance, via multinomial resampling. Let* $\{s_t^j\}_{j=1}^M$ *denote* M *iid draws from a multinomial distribution characterized by support points and weights* $\{\tilde{s}_t^j, \tilde{W}_t^j\}$ *and set* $W_t^j = 1$ *for* $j =, 1 \ldots, M$. *An approximation of* $\mathbb{E}[h(s_t)|Y_{1:t}, \theta]$ *is given by* $\bar{h}_{t,M} = \frac{1}{M}\sum_{j=1}^{M} h(s_t^j) W_t^j$.

3. **Likelihood Approximation.** *The approximation of the log-likelihood function is given by*

$$\ln \hat{p}(Y_{1:T}|\theta) = \sum_{t=1}^{T} \ln\left(\frac{1}{M}\sum_{j=1}^{M} \tilde{w}_t^j W_{t-1}^j\right). \tag{A.5}$$

B Illustration 2: A VAR with Stochastic Volatility

B.1 Prior Specification

Prior for (Φ_1, Φ_2, Σ)**.** We use a Minnesota-type prior for the reduced-form VAR coefficients that appear in the homoskedastic version of the VAR in (21). The specification of the Minnesota prior follows Del Negro and Schorfheide (2012). The prior is indexed by hyperparameters λ_1, λ_2, and λ_3, and is implemented through dummy observations stacked into (Y^*, X^*). We use three sets of dummy observations, written as $Y_j^* = X_j^* \Phi + U_j$:

$$\begin{aligned}
\begin{bmatrix} \lambda_1 \underline{s}_1 & 0 \\ 0 & \lambda_1 \underline{s}_2 \end{bmatrix} &= \begin{bmatrix} \lambda_1 \underline{s}_1 & 0 & 0 \\ 0 & \lambda_1 \underline{s}_2 & 0 \end{bmatrix} \Phi + \begin{bmatrix} u_{11} & u_{12} \\ u_{21} & u_{22} \end{bmatrix}, \\
\begin{bmatrix} \lambda_2 \underline{y}_1 & \lambda_2 \underline{y}_2 \end{bmatrix} &= \begin{bmatrix} \lambda_2 \underline{y}_1 & \lambda_2 \underline{y}_2 & \lambda_2 \end{bmatrix} \Phi + \begin{bmatrix} u_{11} & u_{12} \\ u_{21} & u_{22} \end{bmatrix}, \\
\begin{bmatrix} \underline{s}_1 & 0 \\ 0 & \underline{s}_2 \end{bmatrix} &= \begin{bmatrix} 0 & 0 & 0 \\ 0 & 0 & 0 \end{bmatrix} \Phi + \begin{bmatrix} u_{11} & u_{12} \\ u_{21} & u_{22} \end{bmatrix},
\end{aligned}$$

where $\underline{y}_i$ and $\underline{s}_i$ are the mean and standard deviation of y_i. The first set of dummy observations implies that the VAR coefficients are centered at univariate unit-root representations. The second set of dummy observations implies that if the lagged value y_{t-1} take the value $\underline{y}$, then the current value y_t will be close to $\underline{y}$. The third set of dummy observations induces a prior for the covariance matrix of u_t and is repeated λ_3 times. The dummy observations induce a conjugate MNIW prior for (Φ, Σ):

$$\Sigma \sim IW(\underline{S}, \underline{\nu}), \quad \Phi|\Sigma \sim MN(\underline{\mu}, \Sigma \otimes \underline{P}^{-1}),$$

with

$$\underline{\nu} = T^* - k, \quad \underline{S} = S^*, \quad \underline{\mu} = \Phi^*, \quad \underline{P} = X^{*\prime} X^*,$$

where $\Phi^* = (X^{*\prime} X^*)^{-1} X^{*\prime} Y^*$ and $S^* = (Y^* - X^* \Phi^*)'(Y^* - X^* \Phi^*)$. We set $\lambda_1 = 1$, $\lambda_2 = 1$, and $\lambda_3 = 3$.

Prior for ρ_i**.** The prior for each ρ_i is Uniform on $[0, 1]$.

Prior for ξ_i**.** The prior of ξ_i is specified as an inverse Gamma distribution. It is parameterized as scaled inverse χ^2 distribution with density $p(\xi^2|s^2, \nu) \propto (\xi^2)^{-\nu/2-1} \exp[-\nu s^2/(2\xi^2)]$, where $\sqrt{s^2}$ is 0.3 and ν is 2.0. The density of ξ_i is obtained by the change of variables $\xi = \sqrt{\xi^2}$.

B.2 Further Results for the VAR-SV

Fig. A-1: VAR-SV: Target and Approximate Posterior Densities for DGP 1

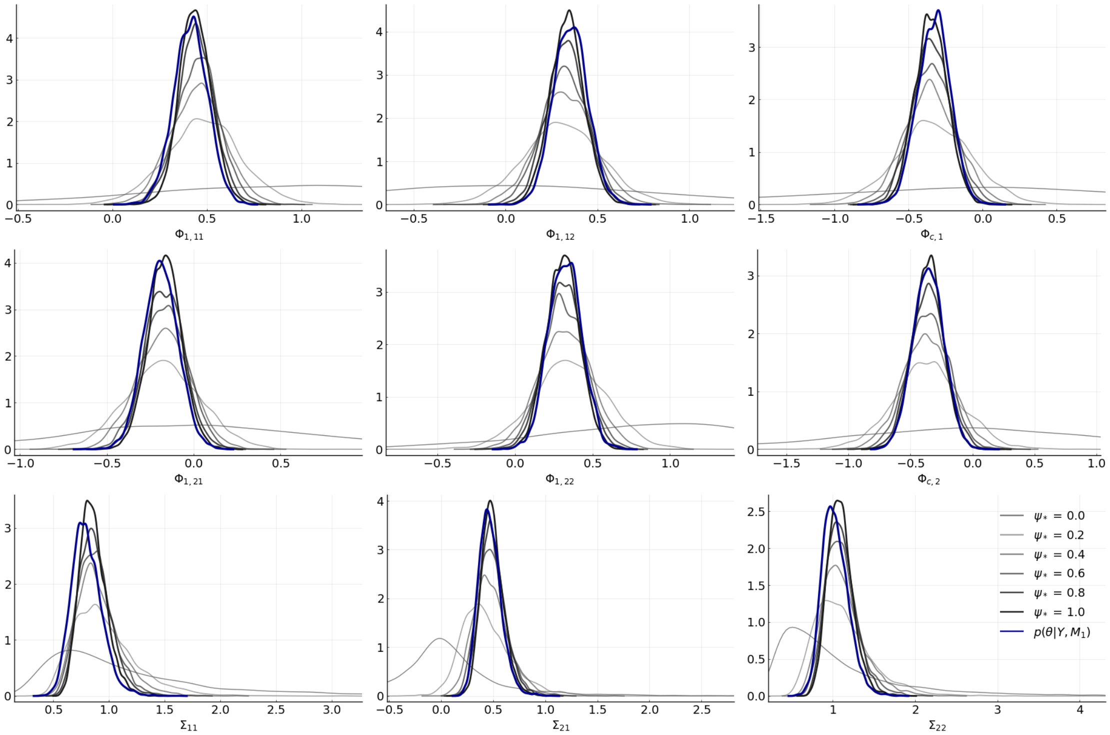

Notes: Each plot refers to a different parameter. The approximating posterior densities obtained from the tempered M_0 likelihood function for $\psi_* \in \{0.0, 0.2, 0.4, 0.6, 0.8, 1.0\}$ are plotted in shades (the larger ψ_* the darker) of gray. The M_1 posterior is depicted in blue. The stochastic volatility parameters $\rho_i, \xi_i,\ i = 1, 2$ are not displayed because model M_0 is uninformative for them.

Fig. A-2: VAR-SV: Target and Approximate Posterior Densities for DGP 2

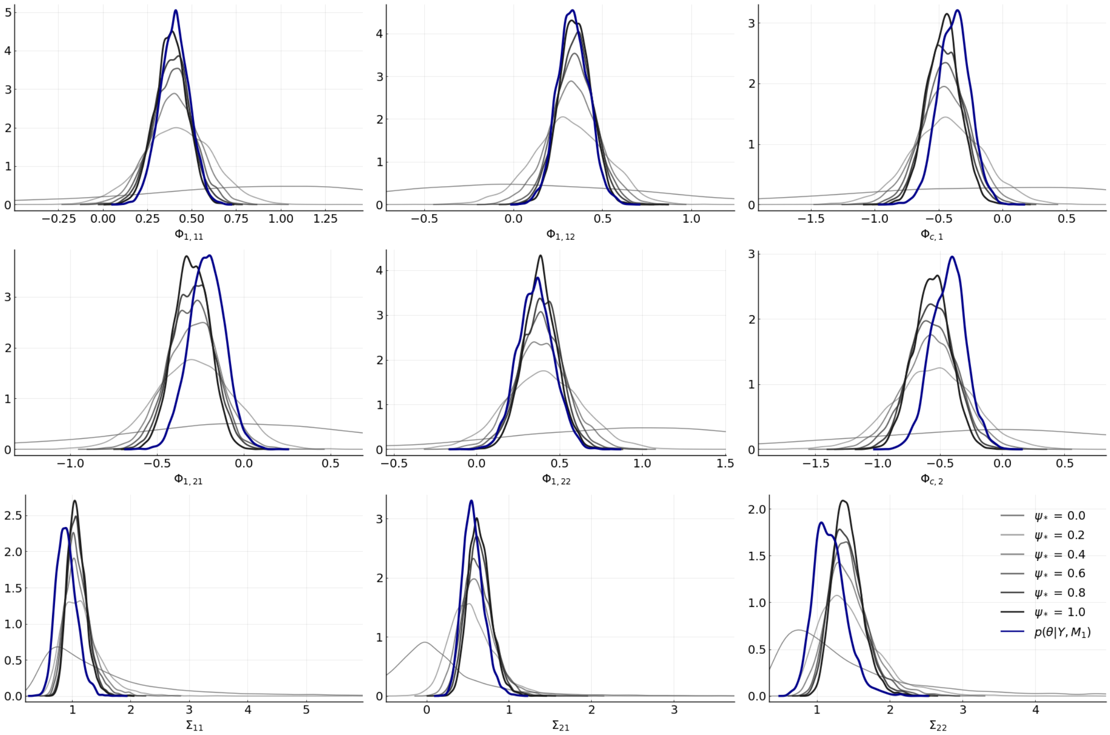

Notes: Each plot refers to a different parameter. The approximating posterior densities obtained from the tempered M_0 likelihood function for $\psi_* \in \{0.0, 0.2, 0.4, 0.6, 0.8, 1.0\}$ are plotted in shades (the larger ψ_* the darker) of gray. The M_1 posterior is depicted in blue. The stochastic volatility parameters $\rho_i, \xi_i,\ i = 1, 2$ are not displayed because model M_0 is uninformative for them.

Fig. A-3: VAR-SV: Target and Approximate Posterior Densities for DGP 3

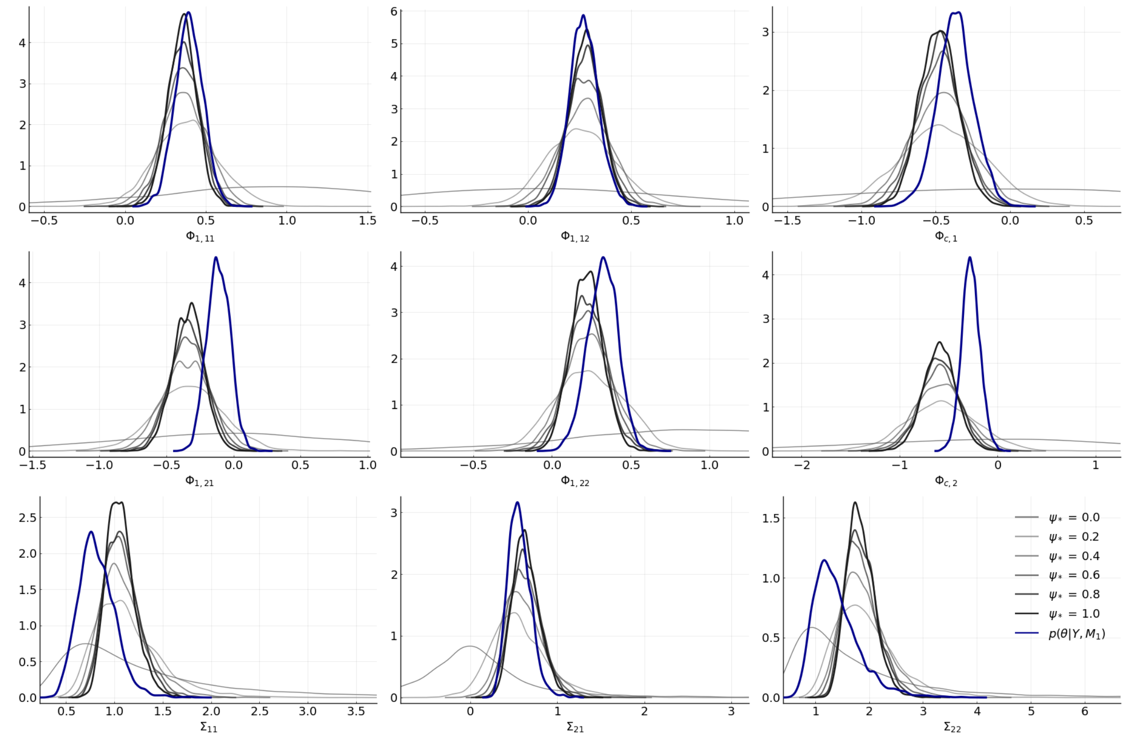

Notes: Each plot refers to a different parameter. The approximating posterior densities obtained from the tempered M_0 likelihood function for $\psi_* \in \{0.0, 0.2, 0.4, 0.6, 0.8, 1.0\}$ are plotted in shades (the larger ψ_* the darker) of gray. The M_1 posterior is depicted in blue. The stochastic volatility parameters $\rho_i, \xi_i,\ i = 1, 2$ are not displayed because model M_0 is uninformative for them.

Fig. A-4: VAR-SV: Monte Carlo Approximations of Posterior Statistics for DGP 1

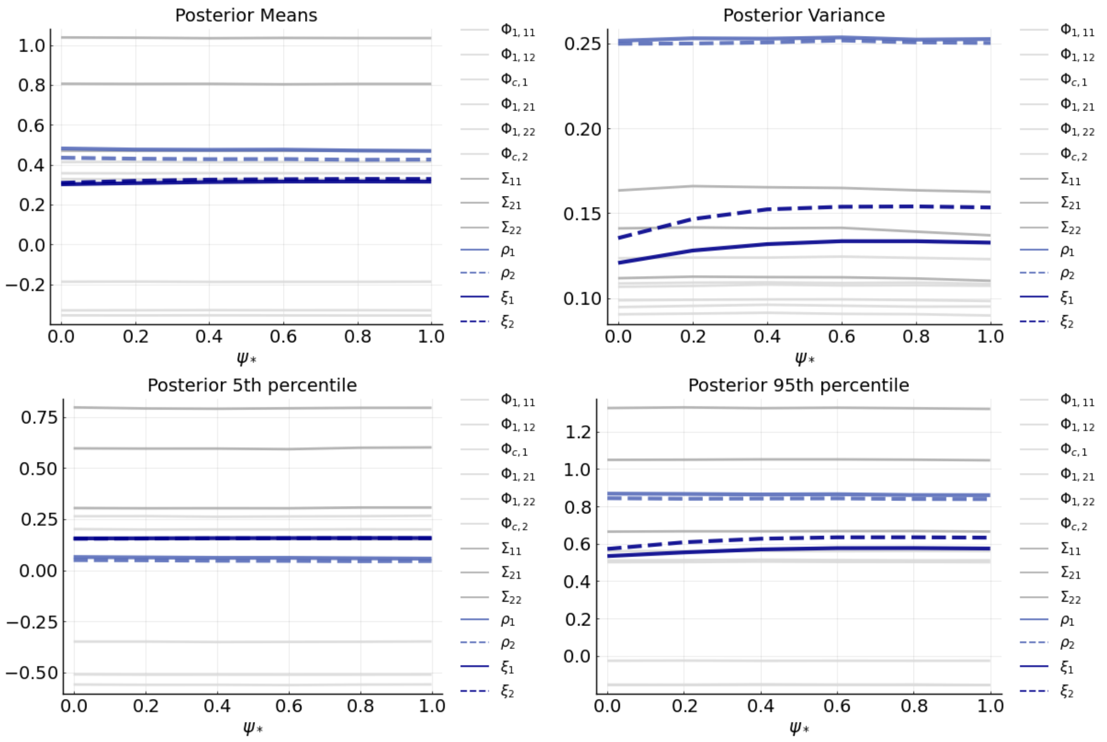

Notes: Each panel shows the Monte Carlo approximation of the respective posterior statistic as a function of the tempering parameter ψ_* for the approximating model. Depicted are means across $N_{run} = 200$ runs.

Fig. A-5: VAR-SV: Runtime and Tempering Schedule

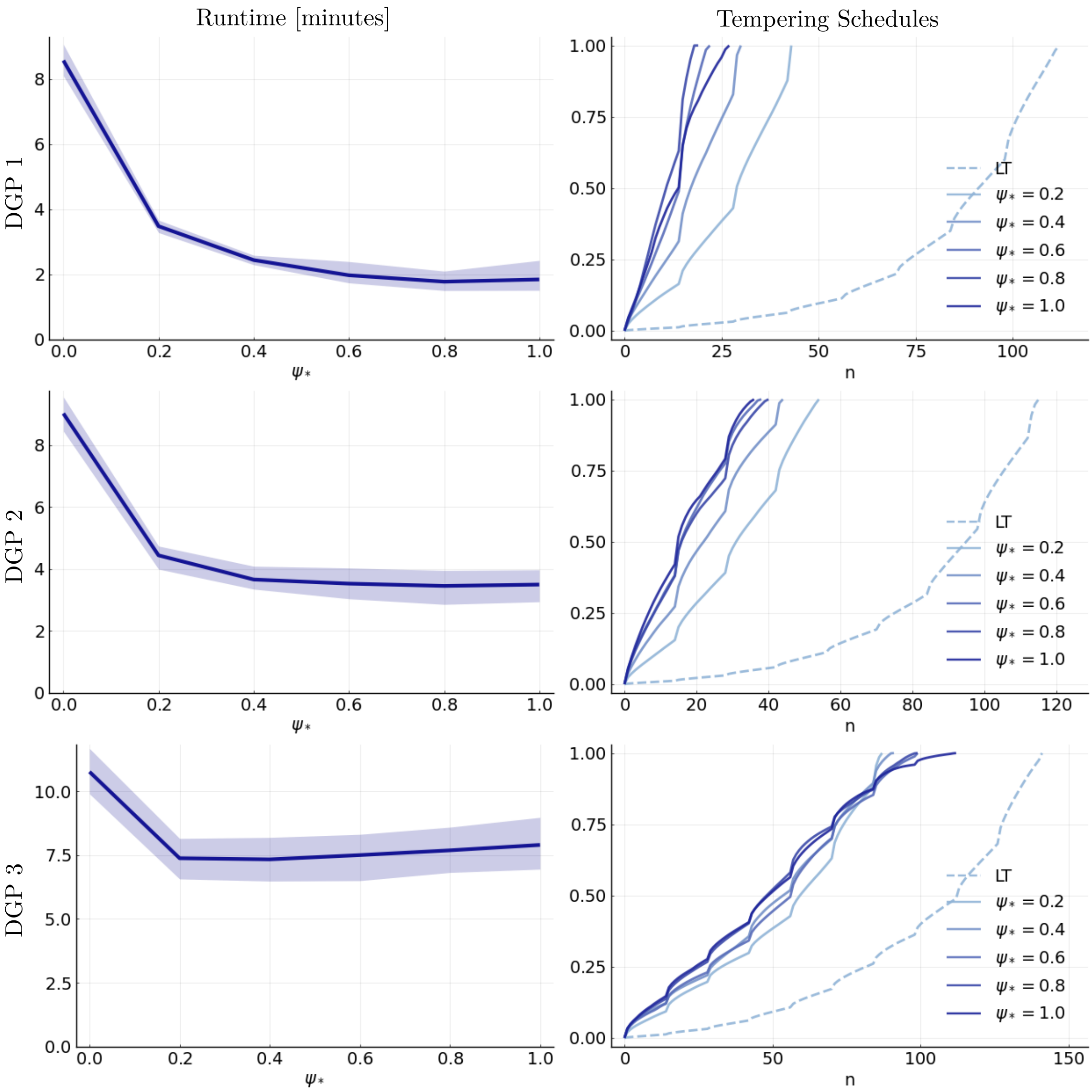

Notes: The left panel shows the mean runtime and 90% confidence interval across $N_{run} = 200$ runs. The right panel illustrates the evolution of the tempering schedule by plotting the median value of the tempering parameter at each stage n.

C Illustration 3: A Nonlinear DSGE Model

C.1 Equilibrium Conditions, Steady State, and Log-linearization

We write the social planner's problem stated in the main text as

$$\begin{aligned} V(K,S) &= \max_{C,L,K'} u(B,C,L) + \beta \mathbb{E}_{S'|S}[V(K',S')] \\ &\text{s.t.} \quad C + I + K\Phi(K'/K) = Y, && \text{(A.6)} \\ &\qquad Y = f(Z,K,L), && \text{(A.7)} \\ &\qquad I = K' - (1-\delta)K\ . && \text{(A.8)} \end{aligned}$$

We use the following functional forms:

$$\begin{aligned} u(B,C,L) &= \frac{C^{1-\tau}-1}{1-\tau} - B\frac{L^{1+1/\nu}}{1+1/\nu}, \\ f(Z,K,L) &= ZK^{\alpha}L^{1-\alpha}, \\ \Phi(K'/K) &= \phi_1\left(\frac{\exp(-\phi_2(K'/K-1)) + \phi_2(K'/K-1) - 1}{\phi_2^2}\right). \end{aligned}$$

The exogenous processes evolve according to:

$$\begin{aligned} Z &= Z_* e^{\hat{z}}, \quad \hat{z}' = \rho_z \hat{z} + \sigma_z \varepsilon_z', \\ B &= B_* e^{\hat{b}}, \quad \hat{b}' = \rho_b \hat{b} + \sigma_b \varepsilon_b'\ . \end{aligned}$$

Throughout this section we use $f_i(\cdot)$ to denote the derivative of a function $f(\cdot)$ with respect to its i'th argument.

C.1.1 First-Order Conditions (FOCs)

Substitute (A.7) and (A.8) into (A.6) and then take FOCs with respect to L and K'. The FOC for L takes the form

$$u_2(B,C,L)f_3(Z,K,L) + u_3(B,C,L) = 0.$$

Using the functional forms, this leads to

$$(1-\alpha)\frac{Y}{L} = BC^{\tau}L^{1/\nu}. \tag{A.9}$$

Now write

$$C = ZK^{\alpha}L^{1-\alpha} - K' + (1-\delta)K - K\Phi(K'/K).$$

The FOC for K' takes the form:

$$-u_2(B,C,L)\big[1 + \Phi_1(K'/K)\big] + \beta\mathbb{E}\left[V_1(K',S')\right] = 0.$$

Plugging in the expressions for $u_2(\cdot)$ and $V_1(\cdot)$ we obtain

$$\begin{aligned} &C^{-\tau}\left[1 + \Phi_1(K'/K)\right] && \text{(A.10)} \\ &\quad = \beta\mathbb{E}\left[C'^{-\tau}\left(\alpha\frac{Y'}{K'} + 1 - \delta - \Phi(K''/K') + \Phi_1(K''/K')\frac{K''}{K'}\right)\right], \end{aligned}$$

where

$$\Phi_1(x) = \frac{\phi_1}{\phi_2}\left[1 - \exp\{-\phi_2(x-1)\}\right]. \tag{A.11}$$

C.1.2 Steady State

Rather than taking (Z_*, B_*) as given and solving for (Y_*, L_*) and the remaining steady states, we proceed in the other direction and solve for (Z_*, B_*) as a function of (Y_*, L_*). Notice that the adjustment costs are zero in steady state because $\Phi(1) = 0$. Moreover, $\Phi_1(1) = 0$. We deduce from (A.10) that

$$\frac{1}{\beta} = \alpha \frac{Y_*}{K_*} + (1-\delta),$$

which implies that

$$K_* = \frac{\alpha}{1/\beta - (1-\delta)} Y_*. \tag{A.12}$$

The capital accumulation equation implies that

$$I_* = \delta K_* = \frac{\alpha\delta}{1/\beta - (1-\delta)} Y_*. \tag{A.13}$$

The aggregate resource constraint implies that

$$C_* = Y_* - I_* = \left(1 - \frac{\alpha\delta}{1/\beta - (1-\delta)}\right) Y_*. \tag{A.14}$$

The production function can be solved for Z_*:

$$Z_* = \frac{Y_*}{K_*^\alpha L_*^{1-\alpha}} = \left(\frac{1/\beta - (1-\delta)}{\alpha}\right)^\alpha \left(\frac{Y_*}{L_*}\right)^{1-\alpha}. \tag{A.15}$$

Finally, we solve (A.9) for B to obtain B_*:

$$B_* = (1-\alpha)\frac{Y_*}{L_*} C_*^{-\tau} L_*^{-1/\nu}.$$

In the numerical illustration we set $Y_* = L_* = 1$.

C.1.3 Log-Linearization

Log-linearizing Equations (A.6), (A.7), (A.8), and (A.9) yields:

$$\hat{y} = \frac{C_*}{Y_*}\hat{c} + \frac{I_*}{Y_*}\hat{i} \tag{A.16}$$

$$\hat{y} = \hat{z} + \alpha\hat{k} + (1-\alpha)\hat{l} \tag{A.17}$$

$$\delta\hat{i} = \hat{k}' - (1-\delta)\hat{k} \tag{A.18}$$

$$(1 + 1/\nu)\hat{l} = \hat{y} - \hat{b} - \tau\hat{c}. \tag{A.19}$$

We proceed with the log-linearization of $\Phi_1(x)$ in (A.11). Differentiating with respect to the argument yields

$$\Phi_{11}(x) = \phi_1 \exp\{-\phi_2(x-1)\}.$$

Log-linearizing around $x = \exp(z) = 1$ leads to the approximation:

$$\Phi_1\big(\exp(z)\big) \approx \Phi_1(1) + \Phi_{11}(1) \cdot 1 \cdot (z - 0).$$

In turn, we can write

$$\Phi_1(K'/K) \approx \phi_1(\hat{k}' - \hat{k}),$$

which shows that the linex adjustment cost function is equivalent, up to second order, to a quadratic adjustment cost function

$$\Phi(K'/K) \approx \frac{\phi_1}{2}\big(K'/K - 1\big)^2.$$

We now turn to the log-linearization of (A.10) using the observation that $\Phi_1(1) = 0$:

$$\begin{aligned} &-\tau C_*^{-\tau}\hat{c} + C_*^{-\tau}\phi_1(\hat{k}' - \hat{k}) \\ &= \; -\tau\beta C_*^{-\tau}(\alpha Y_*/K_* + 1 - \delta)\mathbb{E}[\hat{c}'] + \alpha\beta C_*^{-\tau}\frac{Y_*}{K_*}\mathbb{E}[\hat{y}' - \hat{k}'] + \phi_1\beta C_*^{-\tau}\mathbb{E}[\hat{k}'' - \hat{k}']. \end{aligned}$$

Multiplying by C_*^{τ}, using (A.12), and noting that $\hat{k}'$ is in the information for the conditional expectation $\mathbb{E}[\cdot]$ yields the simplified equation:

$$-\tau\hat{c} + \phi_1(\hat{k}' - \hat{k}) = -\tau\mathbb{E}[\hat{c}'] + \big(1 - \beta(1-\delta)\big)\big(\mathbb{E}[\hat{y}'] - \hat{k}'\big) + \phi_1\beta\big(\mathbb{E}[\hat{k}''] - \hat{k}'\big). \tag{A.20}$$

Equations (A.16) to (A.20) and the laws of motion for $\hat{z}$ and $\hat{b}$ form a linear rational expectations system that determines the dynamics of the model.

After setting $Y_* = L_* = 1$, the measurement equations in (25) can be written as

$$\ln Y^o = \hat{y} + \eta_Y, \quad \ln I^o = \ln\left(\frac{\alpha\delta}{1/\beta - (1-\delta)}\right) + \hat{i} + \eta_I, \quad \ln L^o = \hat{l} + \eta_l. \tag{A.21}$$

C.2 Model Solution, and Computational Details

While the approximate model M_0 refers to a first-order linearization around the steady state and is described in Section C.1 above, we obtain M_1 as a second-order linearization around the steady state, computed following Schmitt-Grohé and Uribe (2004). To implement it in Julia, we use the package *SolveDSGE*, developed by Richard Dennis and available at *https://github.com/RJDennis*.

C.3 Further Results for the RBC Model

Fig. A-6: RBC Model: Simulated Data

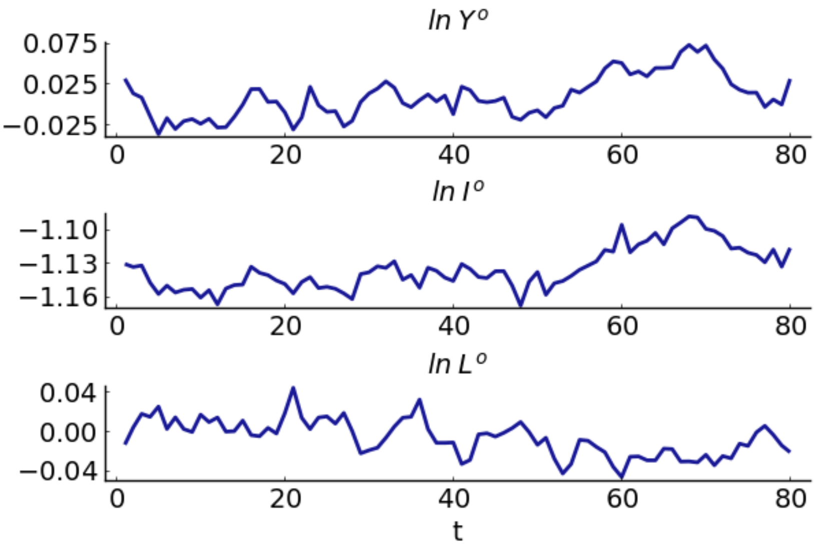

Fig. A-7: RBC Model: Target and Approximate Posterior Densities

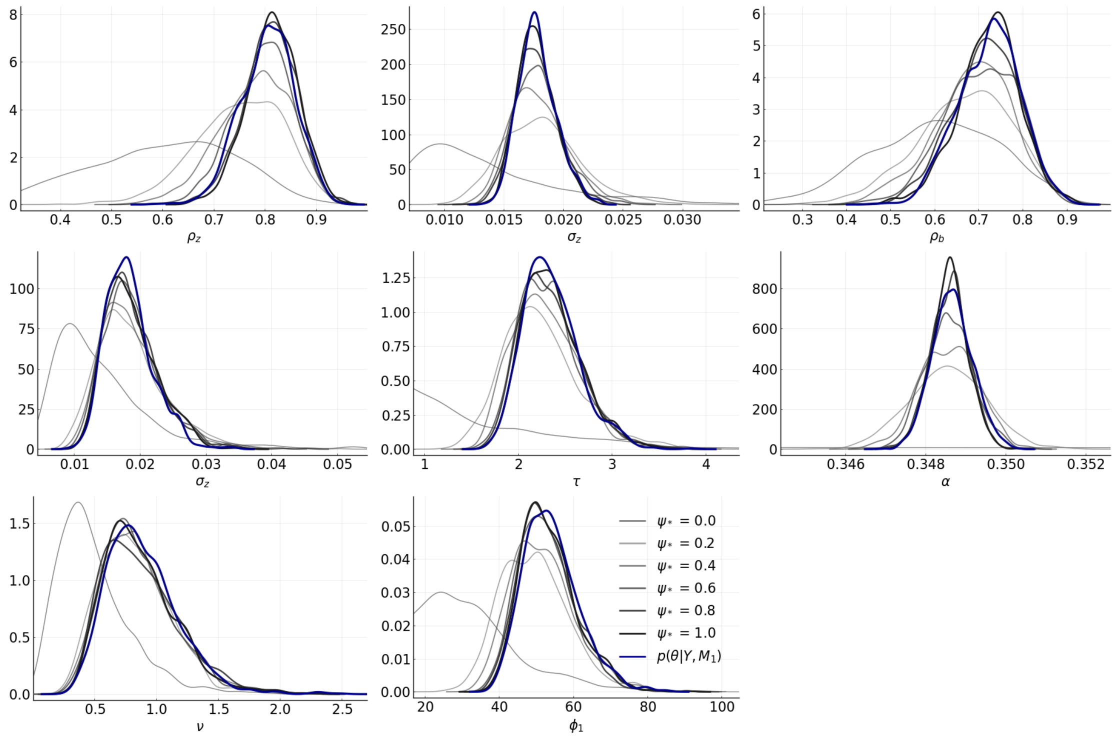

Notes: Each plot refers to a different parameter. The approximating posterior densities obtained from the tempered M_0 likelihood function for $\psi_* \in \{0.0, 0.2, 0.4, 0.6, 0.8, 1.0\}$ are plotted in shades (the larger ψ_* the darker) of gray. The M_1 posterior is depicted in blue.

Fig. A-8: RBC Model: Absolute Runtimes

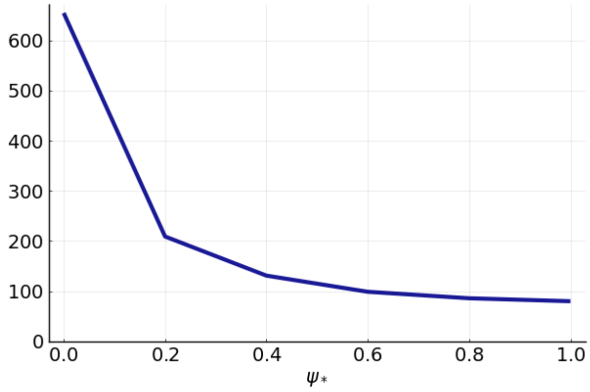

Notes: Absolute runtime as a function of ψ_* based on a single run ($N_{run} = 1$).